7-1-1988

Analysis and Modeling of a Single-Phased Bifilar-Wound Brushless DG Motor

Jeffrey S. Meyer
Purdue University

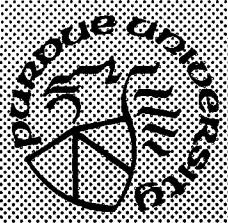

Analysis and Modeling of a Single-Phased Bifilar-Wound Brushless DC Motor

Jeffrey S. Mayer

TR-EE 88-39
July 1988

School of Electrical Engineering
Purdue University
West Lafayette, Indiana 47907

This is dedicated to my family.

ACKNOWLEDGMENTS

Professor Wasynczuk's constant willingness to discuss all aspects of my graduate work is deeply appreciated. I want to thank Professor Krause for encouraging me to pursue graduate work. Special thanks goes to PEPC for its for financial support.

TABLE OF CONTENTS

Page

LIST OF TABLES

LIST OF FIGURES

Figure Page

Figure Page

ABSTRACT

Mayer, Jeffrey S., MSEE, Purdue University, August 1988. Analysis and Modeling of a Single-Phase Bifilar-Wound Brushless DC Machine. Major Professor: Oleg Wasynczuk.

A single-phase brushless dc motor utilizing a bifilar stator winding and having asymmetrical stator pole faces is investigated. The form of the permanent-magnet component of the stator winding flux linkage is analyzed considering the asymmetry of the stator pole faces. Equations describing the electromechanical dynamics of the motor are then derived along with an expression for the electromagnetic torque. The requirements of the dc-to-ac inverter which drives the motor are determined. Using the expression for electromagnetic torque and inverter characteristics, the form of the so-called static electromagnetic torque is analyzed. The so-called cogging torque is established, and in conjunction with the static electromagnetic torque, used to explain the starting characteristics of the motor. The equations for the electromechanical dynamics are converted into state-model form and two mathematical models of the inverter are developed for use in a computer simulation. This computer simulation is then used to demonstrate steady-state and dynamic operation of the motor.

CHAPTER 1
INTRODUCTION

Brushless dc motors are becoming widely used in low-power applications such as blower motors, computer disk drive spindle motors, and in copiers and laser printers [1]. For these applications, the brushless dc motor offers the following advantages: small size, reliability, no carbon dust from brushes, precise speed control, and potentially high efficiency. The most commonly used brushless dc motors are two- or three-phase permanent-magnet synchronous machines driven by a dc-to-ac inverter. The three-phase machine combined with a six-pulse, full-bridge inverter usually represents the best trade-off of machine iron and copper utilization with the cost of the inverter [2]. Because of the prevalence of two- and three-phase devices, they are the brushless dc motors which have been analyzed the most extensively.

On the other hand, there has been little investigation into the operation of the single-phase brushless dc motor. Single-phase motors generally suffer from slow starting characteristics, poor utilization of machine iron and copper, and higher losses. Because of these undesirable characteristics, single-phase motors are limited to applications where rapid response and high efficiency are not required. The lack of general applicability of single-phase motors is, perhaps, the major reason that there has been little investigation into their operation.

The primary advantage offered by single-phase devices is the simplified source requirements. For example, a single-phase brushless dc motor requires only one-third the number of transistors and position sensors needed by a three-phase motor and can be powered by a unipolar voltage supply. Thus, in applications where cost is of greater importance than performance, the single-phase motor may be a superior alternative to a two- or three-phase motor. Examples of applications for which the single-phase motor is well suited are low-flow-rate air blowers used in computer and copying equipment and low-cost computer disk drives.

For the present research, a single-phase bifilar-wound brushless dc motor, designed for use as a computer disk drive spindle motor, is investigated. The investigation encompasses experimental, analytical, and simulation results. The experimental aspects of the research were performed using several identical motors. Experimental data collected from the motors included the winding resistance and inductance and the open-circuit induced voltage created by the rotor permanent magnets. These data were used throughout the analysis and simulation of the motor. A dc-to-ac inverter was designed and built to drive the motor. Measurements of winding currents and voltages during operation of the motor-inverter system provided a benchmark for simulation results. The analytical aspects of the research included: a derivation of the permanent-magnet component of stator winding flux linkage, development of a mathematical model for the motor, determination of the requirements for the dc-to-ac inverter, and an explanation of the self-starting characteristic of the motor. A computer simulation of the motor was developed and used to investigate both steady-state and dynamic operation of

the motor.

In this thesis, Chapter 2 contains a physical description of the device; its distinctive features, a bifilar stator winding and asymmetric stator pole faces, are emphasized. Following the physical description, the permanent-magnet component of stator winding flux linkage is analyzed. The second chapter is concluded with a derivation of the machine's electrodynamic and torque equations. A dc-to-ac inverter designed to drive the brushless dc motor is described in Chapter 3. In Chapter 4, the starting characteristics are analyzed in terms of the so-called static electromagnetic and cogging torques. In Chapter 5, the electrodynamic equations derived in Chapter 2 are expressed in state-model form and two mathematical models for the inverter are developed for use in a computer simulation. Simulations using each model of the inverter are performed and compared to experimental results. Finally, the computer simulation is used to demonstrate the motor's steady-state operation and dynamic performance during starting.

CHAPTER 2
MOTOR DESCRIPTION

2.1 Introduction

In this chapter, a physical description of the single-phase brushless dc motor is provided. In addition, a mathematical model is established which may be used to predict its steady-state and dynamic electromechanical behavior. An important feature of this motor is the asymmetry of its stator pole faces. An analysis of the stator flux linkage which considers the effects of the stator asymmetry is presented and supported by plots of the measured open-circuit induced voltage. Electrodynamic equations relating the stator voltages and currents, and expressions for coupling field energy and electromagnetic torque are then developed. The characterization of the electrical, magnetic, and mechanical systems is completed with measured values of resistance, inductance, and inertia.

2.2 Physical Description

The brushless dc motor analyzed is a four-pole, single-phase, permanent-magnet synchronous machine. There are two stator windings with three terminals; two ends of the stator windings are connected to a common

terminal. This winding arrangement is referred to as a bifilar winding. The stator winding terminals are connected to a dc-to-ac inverter and the combination of the inverter and synchronous machine is referred to as a brushless dc motor. The motor has three distinctive features: a salient-pole asymmetric stator, an external bell-type rotor, and the so-called bifilar stator winding. The salient features of the synchronous machine are described in the following paragraphs, while a detailed description of the inverter is given in the next chapter.

A cross-sectional view of the stator and rotor assembly with the air gap exaggerated for clarity is depicted in Fig. 2.2—1. The internal stator is a 3 mm stack of six steel laminations shaped like the section depicted in Fig. 2.2—1 and has an outer diameter of 53 mm. Four distinct poles extend from a central ring then flair to form pole faces spanning approximately 80°. Some portions of the stator pole faces are augmented with extra steel laminations which rise 2 mm above the rest of the stack. These portions are depicted by double arcs in Fig. 2.2—1 and are more clearly seen in the orthographic view of the stator in Fig. 2.2—2. The stator asymmetry refers to the presence of these raised portions of the stator pole faces. The asymmetry manifests itself in detents (positions for which the rotor as an affinity). The detent positions play an important role in starting of the motor, which is analyzed in Chapter 4. The effects of the stator asymmetry on the stator flux linkage due to the rotor permanent magnets are discussed in the next section.

A uniform air gap separates the stator from the external rotor which, in Fig. 2.2—1, is shown rotated by the angle θ_{rm}. The rotor has four ferrite magnets bonded to the interior of a soft steel cap. The equally sized magnets

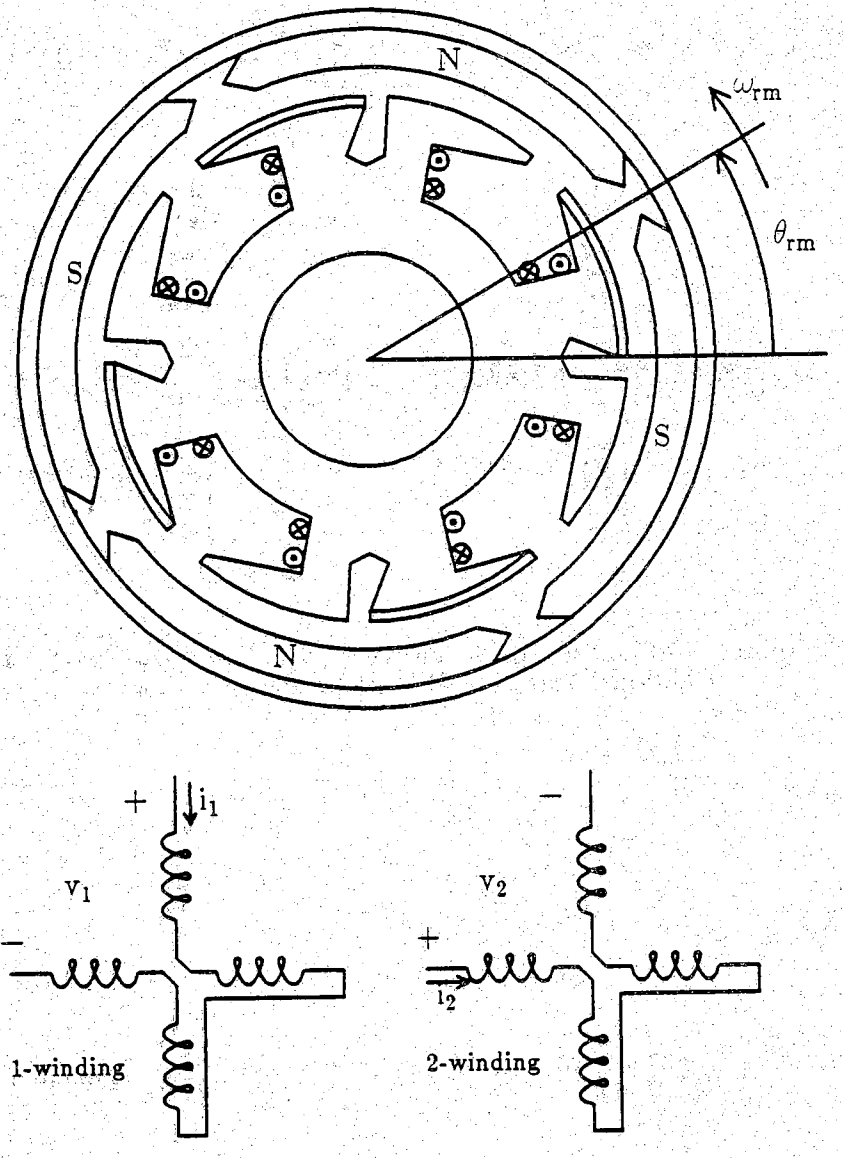

Figure 2.2—1 Cross-sectional view of the stator and rotor assembly and schematic diagram of the bifilar stator winding.

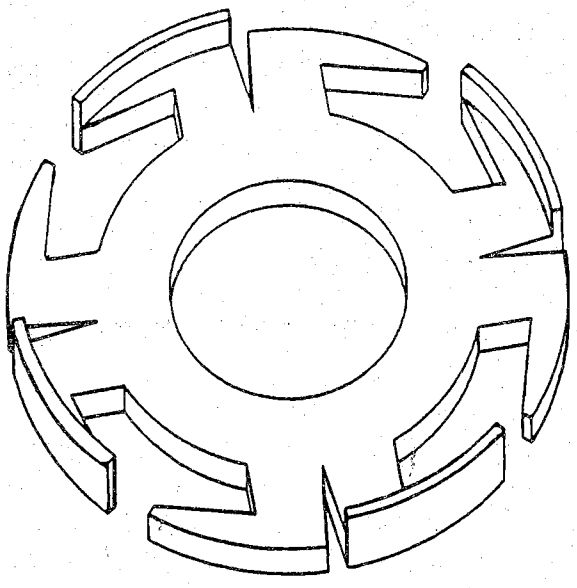

Figure 2.2—2 Orthographic view of the stator.

are arranged such that their interior surfaces alternate north-south-north-south (N-S-N-S). The interior diameter of the rotor surface is 54 mm, leading to a uniform air gap of 0.5 mm. The magnets have an axial length of 6 mm. Here, axial direction is taken as perpendicular to the cross-sectional view. The rotor cap has a 68 mm outer diameter and an axial length of 8 mm. The rotor is supported by a thrust bearing, which fits through the stator central ring.

The bifilar stator winding is depicted in Fig. 2.2—1 by two oppositely directed coil symbols on each stator pole. A coil symbol shows the cross section of one coil turn and indicates a positive direction of current into the page with $\otimes$ and out of the page with $\odot$. The 61-turn coils represented by the outermost coil symbols are series-connected and form a stator winding which will be denoted as the 1-winding. The innermost symbols represent a

second similar winding denoted as the 2-winding. The series connection of the four coils in each winding is more clearly seen in the winding schematic below the cross-sectional view in Fig. 2.2—1. The coils are constructed by winding a pair of conductors around the stator poles. As a result, the two coils on each pole share the same (opposing) magnetic axis and are tightly coupled. Because the machine has a single magnetic axis (for each stator pole), it is a single-phase device. The 1- and 2-windings share a common terminal which is connected to the positive terminal of the power supply; the other terminal of each winding is connected to ground through a switching transistor. The bifilar stator winding and switching circuit (inverter) are depicted in simplified form in Fig. 2.2—3. It should be emphasized that the two windings are actually wound as a pair of conductors around the same steel. However, because the opposite end of each winding is connected to the common terminal, the windings have opposite magnetic sense; positive current in the 1-winding produces magnetic flux which is opposite in direction to the magnetic flux produced by positive current in the 2-winding. The switching signal input to the inverter controls current in the 1-winding; either there is positive current or the winding is open-circuited. The switching signal for the 2-winding is the complement of the 1-winding signal; as a result, there is positive current in only one winding at a time. By alternately supplying a positive current in the two stator windings, an alternating magnetic flux is produced. The bifilar winding combined with this switching circuit has the advantage of requiring only a unipolar voltage source to produce the effect of a bipolar supply.

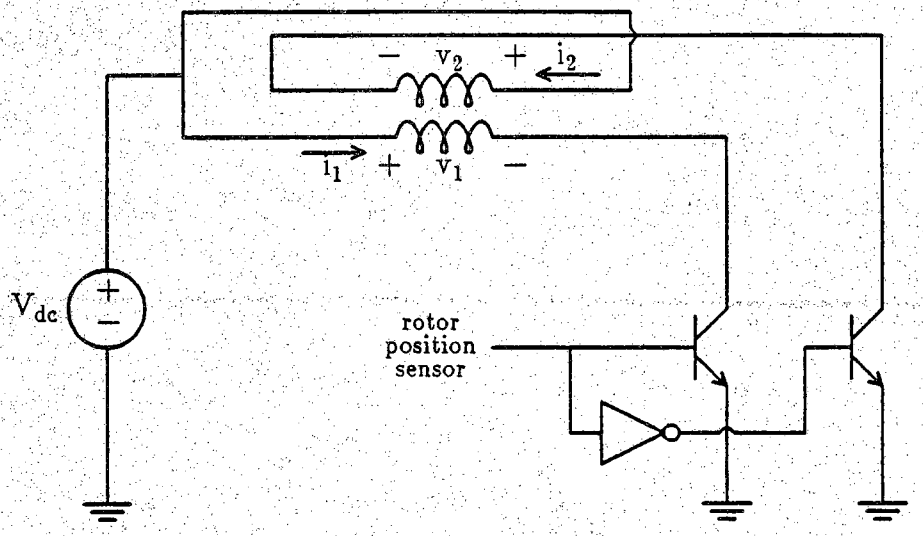

Figure 2.2–3 Simplified schematic diagram of the bifilar stator winding and switching circuit.

The switching signal supplied to the inverter is based upon rotor position. A stationary sensor indicates rotor position by signaling the polarity of the inner surface of the rotor magnet spinning past the sensor. The sensor is mounted on a printed circuit board which lies parallel to the rotor (cross-sectional view). The sensor consists of a Hall-effect element whose output voltage depends upon the magnetic field direction and integrated circuitry to amplify, square, and buffer the sensor's output signal. The resulting output is a TTL compatible logic signal.

2.3 Analytical Derivation of Permanent Magnet Flux Linkage

Prediction of the flux linking the bifilar stator winding due to the rotor permanent magnets serves as a starting point for the analysis of the given brushless dc motor. A distinctive feature of the motor is the stator asymmetry created by differences in axial length (height) of sections of the stator pole faces. The stator asymmetry affects the reluctance of the motor's magnetic circuit and is considered in the following derivation of the flux linking the stator winding due to the permanent magnets.

Although the given brushless dc motor is a four-pole device, it is convenient to consider a two-pole version to facilitate analysis. The equations of the two-pole equivalent device are readily modified with a simple substitution of variables to represent the the actual four-pole motor. A cross-sectional view of the two-pole machine is shown in Fig. 2.3–1. The two stator poles extend from a single stator section, rather than from the central stator ring. Wound around each stator pole are two coils, one for each of the two stator windings which comprise the bifilar winding. In Fig. 2.3–1, coils 1_a–$1_a'$ and 1_b–$1_b'$ are series-connected forming the 1-winding. Similarly, coils 2_a–$2_a'$ and 2_b–$2_b'$ coils form the the 2-winding. Positive current in the 1-winding (both the 1_a–$1_a'$ and 1_b–$1_b'$ coils) produces positive flux horizontally to the right; an axis in that direction is shown and labeled as the 1–axis. Position on the stator is measured by the stator displacement ϕ_s from the 1–axis. The rotor quadrature-axis (q–axis) extends outward from the center of the rotor between the north (N) and south (S) permanent magnets. Rotor position is indicated by the angle θ_r, measured between the 1–axis and q–axis, while points on the rotor are located by the rotor displacement ϕ_r measured from the

q—axis. A position on the rotor may also be measured relative to the 1—axis using the relationship $\phi_s = \theta_r + \phi_r$.

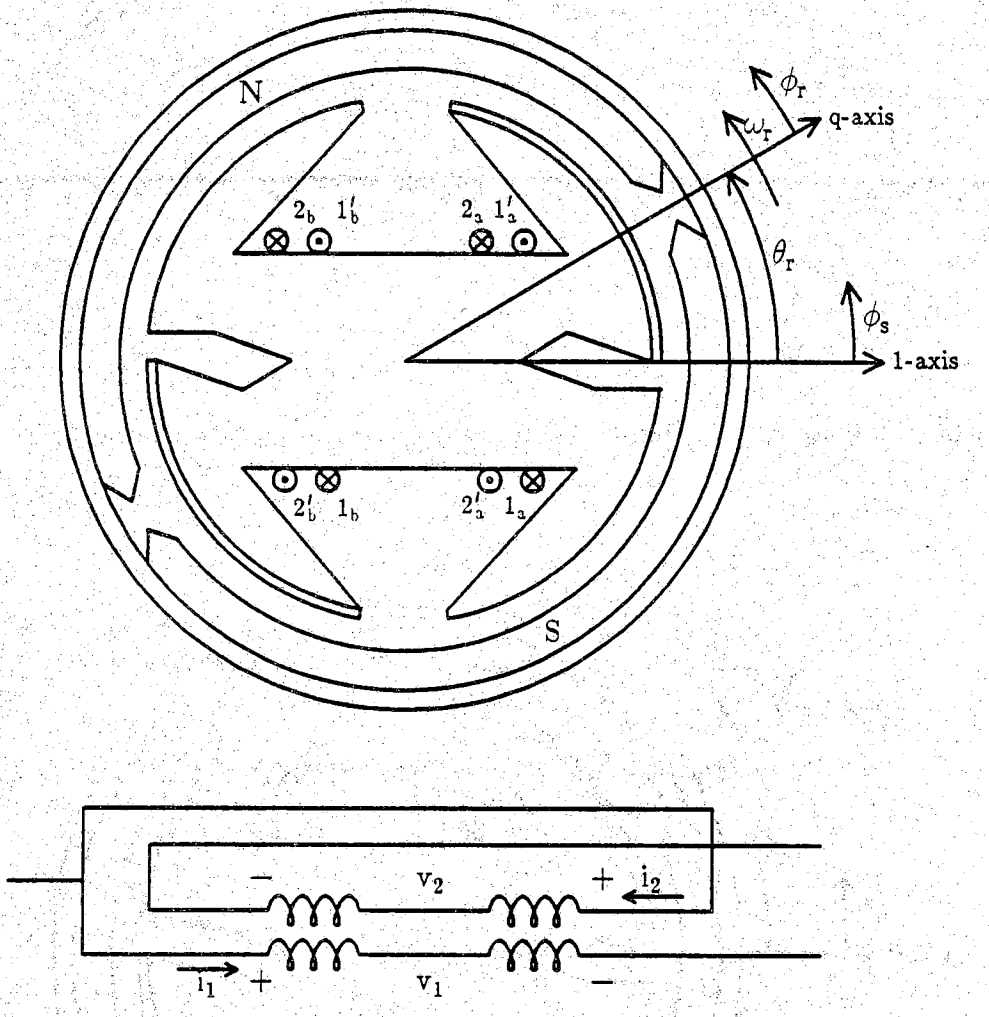

Figure 2.3—1 Cross-sectional view of the two-pole machine.

The analysis of stator flux linkage due to the rotor permanent magnets begins with a description of the machine's magnetic circuit. The topology of the magnetic circuit depends upon rotor position. Two extreme rotor

positions, the stator and rotor poles aligned and the stator and rotor poles unaligned, are shown in Fig. 2.3–2. The dashed lines in Fig. 2.3–2 depict magnetic flux lines. Flux crossing the air gap from the rotor north pole is primarily radial because the uniform air gap is small relative to the axial length of the permanent magnets (about one-twelfth the length). The non-radial components of flux in the stator and rotor steel and in the space above and below the stator stack are inconsequential when considering the effects of the air-gap flux. Flux issuing from the rotor north pole which passes through a stator pole face is channeled within the highly permeable stator steel through the coils, thereby linking the coils on that pole. With the stator and rotor poles aligned, as in Fig. 2.3–2(a), the flux issuing from the rotor north pole and crossing the air gap into the stator links the coils on both stator poles and crosses the air gap again toward the rotor south pole. With the stator and rotor poles unaligned, as in Fig. 2.3–2(b), the flux entering the upper-left pole face will return to the rotor south pole without linking the winding. The total flux linking a turn of the stator winding is equal to the net flux entering both halves of the left pole face. Flux which does not pass through a pole face does not link the winding because of the low relative permeability of the air and the location of the spaces between the stator pole faces.

An expression for the stator winding flux linkage due to the rotor permanent magnets is obtained by multiplying the flux through a single winding turn by the total number of turns in the winding. In order to simplify references to windings, the single turn considered will be that shown for the 1_a–$1_a'$ coil in Fig. 2.3–1. With a change in sign, the results obtained for the 1-winding apply to the 2-winding. The permanent-magnet flux linking a single

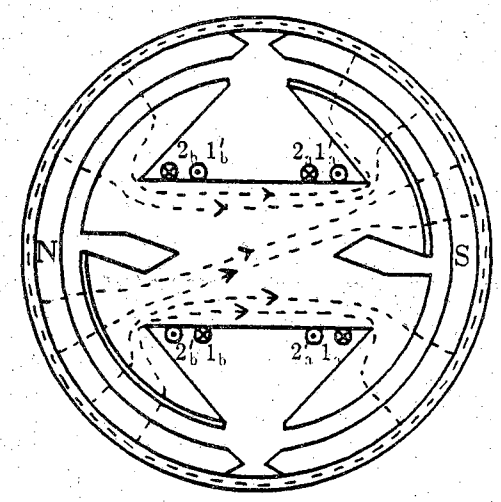

(a)

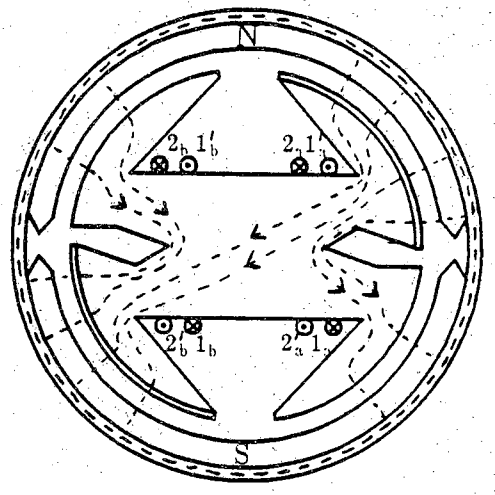

(b)

Figure 2.3—2 The magnetic circuit when the stator and rotor poles are (a) aligned ($\theta_r = 90^\circ$) and (b) unaligned ($\theta_r = 0^\circ$).

turn of the 1-winding may be expressed

$$\Phi_{pm1} = \int_S \vec{B} \cdot d\vec{S} \tag{2.3-1}$$

where the surface S, over which the integration is performed, may be chosen to be any open surface that has the single turn of the 1-winding as its periphery (boundary). The flux density, $\vec{B}$ in (2.3-1), depends implicitly on the location of the differential surface element, $d\vec{S}$. In addition, because the flux density, $\vec{B}$, varies as a function of the position of the permanent magnets, the flux density and, consequently, flux linkage are functions of rotor position, θ_r. Multiplying the flux through a single winding turn, Φ_{pm1}, by the total number of winding turns produces an expression for flux linkage

$$\lambda_{pm1} = N \int_S \vec{B} \cdot d\vec{S} \tag{2.3-2}$$

The integral of (2.3-2) can be simplified by considering the surface of integration, S, and flux density, $\vec{B}$, in terms of the magnetic circuit description. It was reasoned that flux passing through the stator pole faces links the stator winding. As a result, the right pole face in Fig. 2.3–1 will be used as the open surface of integration, instead of the simpler planar surface bounded by a turn of the 1_a–$1_a'$ coil. The pole face has a uniform radius, r_0, and spans an angle from $\phi_s = \phi_{s0}$ to $\phi_s = \phi_{s1}$. The axial length of the pole face is a function of the stator displacement; a plot of axial length versus stator displacement, $\ell(\phi_s)$, is shown in Fig. 2.3–3(a). Expressing $d\vec{S}$ in terms of $\ell(\phi_s)$, r_0, $d\phi_s$, and $\vec{a}_r$ yields

$$\lambda_{pm1}(\theta_r) = N \int_{\phi_{s0}}^{\phi_{s1}} \vec{B}(\phi_s, \theta_r) \cdot \ell(\phi_s)\, r_0\, d\phi_s\, \vec{a}_r \tag{2.3-3}$$

where $\vec{B}$ is expressed as a function of ϕ_s and θ_r, and λ_{pm1} is expressed as a

function of θ_r. The assumption that the air-gap flux density is radial, $\vec{B} = B_r\vec{a}_r$, allows the dot product in (2.3-3) to be replaced by scalar multiplication

$$\lambda_{pm1}(\theta_r) = N\int_{\phi_{s0}}^{\phi_{s1}} B_r(\phi_s,\theta_r)\,\ell(\phi_s)\,r_0\,d\phi_s \qquad (2.3\text{-}4)$$

The functional dependence of the radial flux density, B_r, on stator location, ϕ_s, and rotor position, θ_r, can be shown explicitly. Recall that the flux density, B_r, is produced by the rotor permanent magnets; an approximation of the distribution of flux density as a function of rotor displacement, $B_r(\phi_r)$, is shown in Fig. 2.3–3(b). The north pole occupies the region, $0 < \phi_r < \pi$, flux from that magnet is radially inward and that region in Fig. 2.3–3(b) is shown as negative. From Fig. 2.3–1, $\phi_r = \phi_s - \theta_r$. Thus, $B_r(\phi_s,\theta_r)$ may be established from $B_r(\phi_r)$, plotted in Fig. 2.3–3(b), by replacing the argument ϕ_r with $\phi_s - \theta_r$. In this case, (2.3-4) may be expressed

$$\lambda_{pm1}(\theta_r) = N\int_{\phi_{s0}}^{\phi_{s1}} B_r(\phi_s-\theta_r)\,\ell(\phi_s)\,r_0\,d\phi_s \qquad (2.3\text{-}5)$$

where $B_r(\cdot)$ is defined in Fig. 2.3–3(b) in terms of ϕ_r.

Using the functions, $\ell(\phi_s)$ and $B_r(\cdot)$, and appropriate values for r_0 and N, the convolution-like definite integral in (2.3-5) can be evaluated numerically over a range of θ_r. A plot of λ_{pm1} versus θ_r is given in Fig. 2.3–4(a). Taking the derivative of $\lambda_{pm1}(\theta_r)$ with respect to θ_r yields the plot in Fig. 2.3–4(b). The derivative, $\dfrac{d\lambda_{pm1}(\theta_r)}{d\theta_r}$, is significant because it appears in the expression for electromagnetic torque developed later and can be experimentally obtained

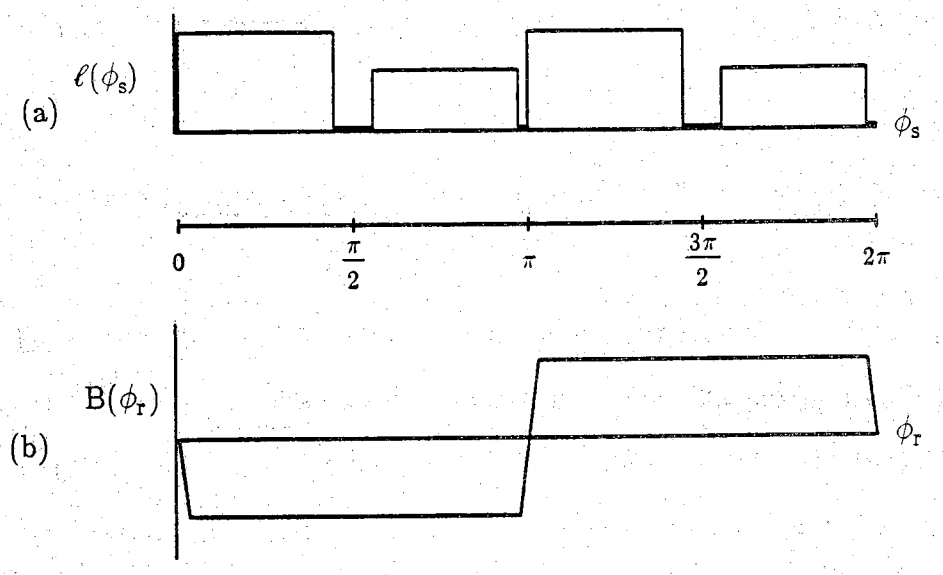

Figure 2.3—3 Plot of (a) stator axial length and (b) approximate flux density distribution.

by dividing the measured open-circuit induced voltage (back emf) by the rotor speed.

The assumptions and simplifications used in the analysis appear justified when the results are compared to measurements. The open-circuit induced voltage (back emf) for a mechanically driven motor is shown in Fig. 2.3—5(a). Integrating the measured emf waveform gives the flux linkage shown in Fig. 2.3—5(b). Comparison with the analytically established results in Fig. 2.3—4 reveals excellent agreement.

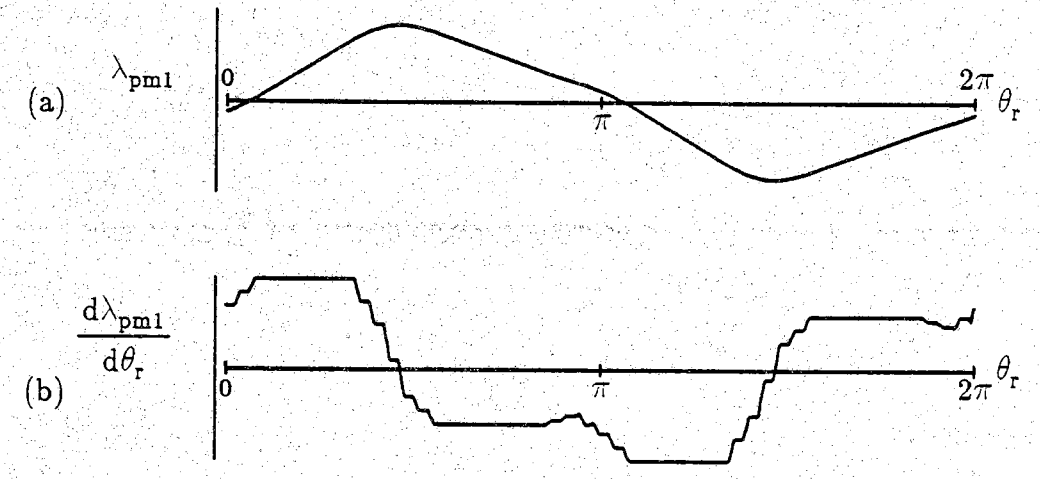

Figure 2.3—4 Analytically derived plot of (a) the permanent-magnet component of flux linkage and (b) its derivative with respect to rotor position.

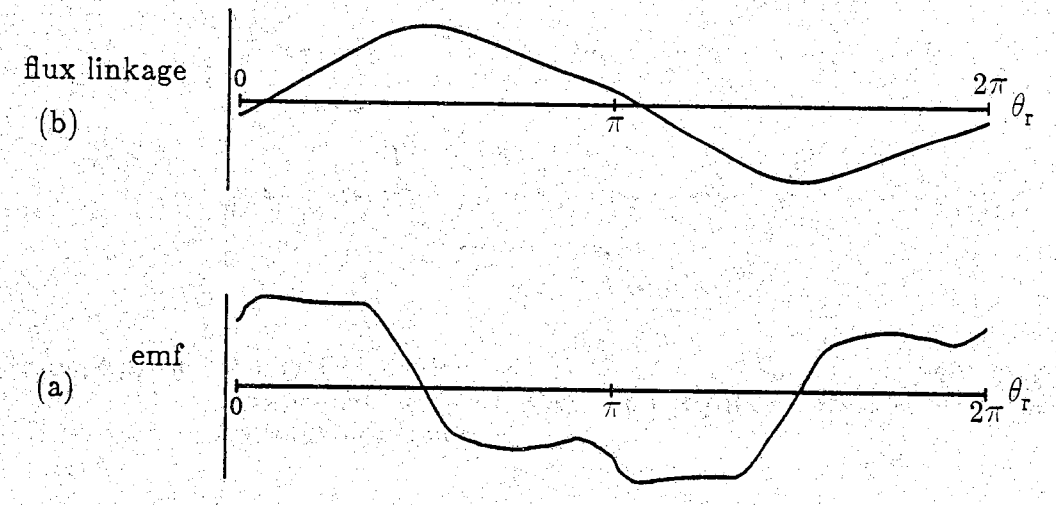

Figure 2.3—5 Experimentally recorded plot of (a) open-circuit induced voltage and (b) its integral.

2.4 Mathematical Model

In this section, a mathematical model of the single phase brushless dc motor, capable of predicting its steady-state and transient response, is derived. This model consists of differential equations describing the dynamics of the electrical and mechanical systems and an algebraic expression for the electromagnetic torque, which mathematically couples the two systems.

The electrical system dynamics may be described by two equations, one for each stator winding, which relate voltages, currents, and changes in flux linkage. From Faraday's law, the induced voltage across each stator winding is equal to the time rate of change of flux linkage. Taking into account the resistance of the stator winding, the applied stator voltages may be expressed

$$v_1 = r_1 i_1 + p\lambda_1 \tag{2.4-1}$$

$$v_2 = r_2 i_2 + p\lambda_2 \tag{2.4-2}$$

where p is the Heaviside notation for the time differentiation operator $\frac{d}{dt}$. Assuming that the stator flux linkages are linearly related to the currents, the winding flux linkages, λ_1 and λ_2, may be expressed in terms of self- and mutual inductances multiplied by currents and a permanent-magnet component of flux linkage, i.e.

$$\lambda_1 = L_{11} i_1 + L_{12} i_2 + \lambda_{pm1} \tag{2.4-3}$$

$$\lambda_2 = L_{21} i_1 + L_{22} i_2 + \lambda_{pm2} \tag{2.4-4}$$

Measurements confirmed the assumption that the stator windings are symmetric. They have the same total self-inductance, resistance, and number

of turns. Since the self-inductance is the same for both windings, L_{11} and L_{22} in (2.4-3) and (2.4-4) will hereafter be denoted as L_{ss}. Since the stator windings are tightly wound on highly permeable stator steel, the numerical value of the mutual inductance is nearly equal to the total self-inductance. However, since the magnetic axes are in opposite directions for positive current in each winding, the mutual inductance is negative. A minus sign and the symbol L_m will replace L_{12} and L_{21} in (2.4-3) and (2.4-4). The symmetry and configuration of the windings indicate that both have the same permanent-magnet component of flux linkage but with opposite signs. The symbol λ_m will be used for the permanent-magnet flux linkage term; a positive sign for the 1-winding is chosen arbitrarily. With these substitutions, the resulting expressions for stator flux linkages become

$$\lambda_1 = L_{ss} i_1 - L_m i_2 + \lambda_m \tag{2.4-5}$$

$$\lambda_2 = - L_m i_1 + L_{ss} i_2 - \lambda_m \tag{2.4-6}$$

The values for the winding parameters (resistances and inductances) were measured experimentally. The measured value of stator resistance, r_s, is $3.7\,\Omega$. The copper windings demonstrated expected thermal characteristics. In particular, resistance increased with temperature, but remained less than $4.1\,\Omega$ even under load. Skin effect at the normal operating frequency (120 Hz) is negligible. Transformer open-circuit and short-circuit tests were performed to determine the stator winding self- and mutual inductances. In the open-circuit test, a sinusoidal voltage was applied to the 1-winding while the 2-winding was open-circuited. Waveforms of the 1-winding voltage and current were recorded

simultaneously and used to determine a voltage phasor and a current phasor, respectively. The ratio of the voltage phasor to the current phasor indicated that the self-inductance, L_{ss}, is 2.4 mH. Using 2.4 mH for the self-inductance and data collected with the 2-winding short-circuited, impedance calculations indicated that the mutual inductance, L_m, is 2.3 mH.

The final form of the electrical dynamic equations and the values for its parameters are

$$v_1 = r_s i_1 + L_{ss} p i_1 - L_m p i_2 + p\lambda_m \tag{2.4-7}$$

$$v_2 = r_s i_2 - L_m p i_1 + L_{ss} p i_2 - p\lambda_m \tag{2.4-8}$$

Table 2.4–1 Electrical system parameters.

r_s	L_{ss}	L_m
3.7 Ω	2.4 mH	2.3 mH

The mechanical dynamics may be described using Newton's second law applied to rotational systems. The torque developed by the electromagnetic system is countered by the inertial acceleration torque, the torques due to windage and friction, and the load torque, i.e.

$$T_e = Jp\omega_r + B\omega_r + T_L \tag{2.4-9}$$

An expression for the electromagnetic torque, T_e, will be developed subsequently. The term $Jp\omega_r$ represents the accelerating torque which is

needed to change the angular velocity of the moment of inertia of the motor and connected load. Manufacturer's specifications list the moment of inertia of the motor as $1.70\,\mu kg{\cdot}m^2$. It will be assumed that windage and friction for the motor can be modeled as a torque which is proportional to angular velocity. The proportionality constant, B, is used for both the windage and friction; its value will be determined from considerations during simulation. The load torque, T_L, represents an externally applied torque which, if negative, accelerates the motor. The load torque will be considered as a mechanical input during simulation of the motor.

The interaction of currents in the stator electrical system with the magnetic field of the rotor permanent magnets creates an electromagnetic torque. An expression for the electromagnetic torque may be derived by first expressing the field energy and then the coenergy [3]. For a two winding system, the field energy may be expressed

$$W_f(i_1,i_2,\theta_r) = \int_0^{i_1} \xi \frac{\partial \lambda_1(\xi,i_2,\theta_r)}{\partial \xi} d\xi + \int_0^{i_2} [i_1 \frac{\partial \lambda_1(i_1,\xi,\theta_r)}{\partial \xi} + \xi \frac{\partial \lambda_2(i_1,\xi,\theta_r)}{\partial \xi}] d\xi + W_{pm}(\theta_r) \qquad (2.4\text{-}10)$$

The first term on the right-hand side of (2.4-10) represents the coupling field energy contributed by current in the 1-winding. The second term is analogous for the 2-winding. The third term represents the coupling field energy contributed by the permanent magnet. The functional dependence of λ_1 and λ_2 on i_1, i_2, and θ_r in (2.4-10) is shown explicitly for clarity. Substituting the

expressions for flux linkages, (2.4-5) and (2.4-6), into (2.4-10) and taking the partial derivatives

$$W_f(i_1,i_2,\theta_r) = \int_0^{i_1} \xi L_{ss}\, d\xi + \int_0^{i_2} i_1(-Lm)\, d\xi + \int_0^{i_2} \xi L_{ss}\, d\xi + W_{pm}(\theta_r) \qquad (2.4\text{-}11)$$

Evaluating the given integral

$$W_f(i_1,i_2,\theta_r) = \frac{1}{2} L_{ss} i_1^2 - L_m i_1 i_2 + \frac{1}{2} L_{ss} i_2^2 + W_{pm}(\theta_r) \qquad (2.4\text{-}12)$$

For a two winding system, the coenergy may be expressed in terms of the field energy as

$$W_c(i_1,i_2,\theta_r) = i_1 \lambda_1(i_1,i_2,\theta_r) + i_2 \lambda_2(i_1,i_2,\theta_r) - W_f(i_1,i_2,\theta_r) \qquad (2.4\text{-}13)$$

Substituting the expressions for the flux linkages, (2.4-5) and (2.4-6), and for the field energy, (2.4-12), into (2.4-13) yields

$$W_c(i_1,i_2,\theta_r) = i_1 [L_{ss} i_1 - L_m i_2 + \lambda_m] + i_2 [-L_m i_1 + L_{ss} i_2 - \lambda_m]$$
$$- \left[\frac{1}{2} L_{ss} i_1^2 - L_m i_2 i_1 + \frac{1}{2} L_{ss} i_2^2 + W_{pm}(\theta_r)\right] \qquad (2.4\text{-}14)$$

Simplifying:

$$W_c(i_1,i_2,\theta_r) = \frac{1}{2} L_{ss} i_1^2 + \frac{1}{2} L_{ss} i_2^2 - L_m i_1 i_2 + (i_1 - i_2)\lambda_m - W_{pm} \qquad (2.4\text{-}15)$$

Finally, the electromagnetic torque is established by taking the partial derivative of the coenergy with respect to rotor position. In particular,

$$T_e = (i_1 - i_2)\frac{\partial \lambda_m}{\partial \theta_r} - \frac{\partial W_{pm}}{\partial \theta_r} \qquad (2.4\text{-}16)$$

Since λ_m and W_{pm} are functions only of θ_r, the partial derivatives in (2.4-16)

may be replaced by total derivatives, i.e.

$$T_e = (i_1 - i_2)\frac{d\lambda_m}{d\theta_r} - \frac{dW_{pm}}{d\theta_r} \tag{2.4-17}$$

The first term on the right-hand side of (2.4-17) represents the electromagnetic torque produced by the interaction of electric current in the stator windings with the magnetic field of the rotor permanent magnets. The second term represents a torque that is due to the attraction between the rotor permanent magnets and the stator steel and acts to drive the rotor to a position having the lowest permanent-magnet component of coupling field energy. This torque ensures that the rotor position of the unexcited motor is such that an electromagnetic torque sufficient for starting is developed when the stator windings are suddenly energized. Chapter 4 is devoted to the issue of starting torque.

CHAPTER 3
INVERTER DESCRIPTION

3.1 Introduction

In a brushless dc motor, a dc-to-ac inverter supplies the stator windings of a permanent-magnet synchronous machine with a set of ac voltages whose frequency corresponds to the rotor speed. In this chapter, an inverter designed for the given brushless dc motor is described. The description is broken into two parts. In the first part, the operation of the inverter's switching transistors and the requirements for the Zener diodes which protect the transistors are presented. The logic which generates the gating signals for the switching transistors is described in the second part.

3.2 Operation of the Inverter

The purpose of the dc-to-ac inverter for the given brushless dc motor is to supply the bifilar stator winding (1- and 2-windings) with a set of ac voltages whose frequency corresponds to the rotor speed. An inverter designed for the present research, connecting the bifilar stator winding to a dc voltage supply, is shown in Fig. 3.2–1. Each leg of the inverter is series-connected to one of the stator windings. The operating characteristics of each inverter leg are

identical. For convenience, equations in the following analysis are written for the leg connected to the 1-winding, but are equally valid, with an appropriate change of subscripts, for the leg connected to the 2-winding.

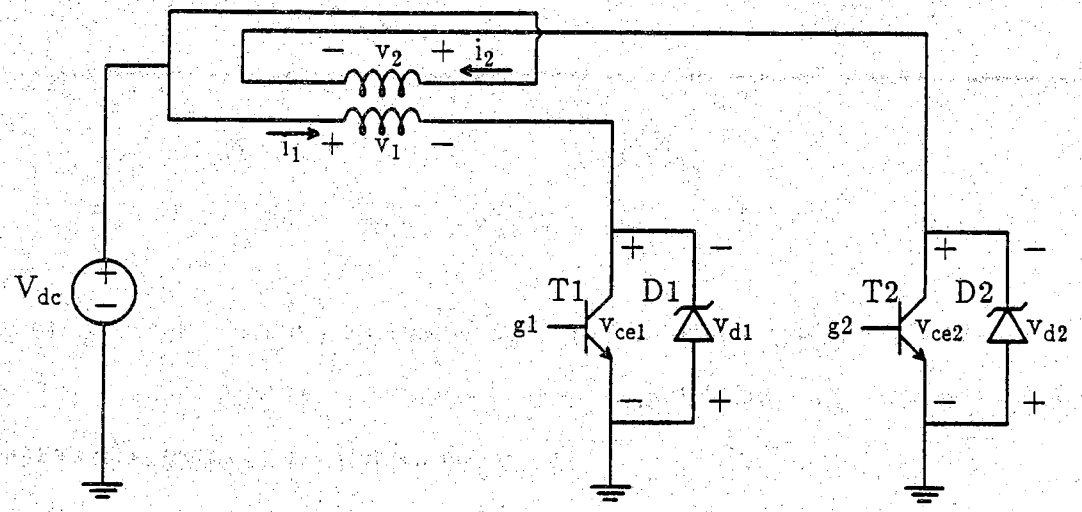

Figure 3.2–1 Schematic diagram of the dc-to-ac inverter and bifilar stator winding.

The bipolar transistors, T1 and T2, are operated as switches that control the voltage (current) supplied to the 1- and 2-winding, respectively. The transistors are driven into saturation (on) or cutoff (off) by the gating signals g1 and g2 which are generated by a switching logic circuit described in the next section. When the gating signal to a transistor is high, the transistor is on and the voltage applied to the winding is approximately equal to the dc supply voltage, $v_1 \approx V_{dc}$; a small collector-to-emitter saturation voltage, $v_{ce}^{sat} \approx 0.25$ V, which lowers the applied stator voltage, will be considered in subsequent analyses. When the gating signal to a transistor is low, the

transistor is off and the winding is essentially open-circuited, $i_1 = 0$. A positive open-circuit voltage, induced by the time rate of change of the 2-winding current, pi_2, and the permanent-magnet flux linkage, $p\lambda_m$, appears across the transistor (diode). Generally, the gating signals are complementary; when one is high, the other is low and vice versa. During the so-called commutation interval, however, both signals are momentarily low; that is, the low-to-high transition of one signal is delayed relative to the high-to-low transition of the other. More information about the gating signals will be given in the next section.

The Zener diodes, D1 and D2, connected between the emitter and collector terminals of transistors T1 and T2 protect the transistors during commutation. The Zener voltage, V_z, is considered to be a positive constant value and is selected to be less than the transistors' collector-to-emitter breakdown voltage, V_{ce}^{break}, and greater than twice the dc supply voltage, V_{dc}. In particular, $V_{ce}^{break} > V_z > 2V_{dc}$. These bounds are determined by analyzing the voltage developed across transistor T1 during the intervals in which that transistor is being commutated off or is already off. An equation for the collector-to-emitter voltage, v_{ce1}, is obtained from Kirchoff's voltage law applied to the loop containing transistor T1, the dc voltage supply, and the 1-winding, i.e.

$$v_{ce1} = V_{dc} - v_1 \tag{3.2-1}$$

Substituting (2.4-7) for the 1-winding voltage, v_1, yields

$$v_{ce1} = V_{dc} - ri_1 - L_{ss}pi_1 + L_m pi_2 - p\lambda_m \tag{3.2-2}$$

A value for v_{ce1} during the interval in which transistor T1 is being commutated off can be estimated from (3.2-2). Observations revealed that during

commutation, the algebraic sum of the first, second, and last terms on the right-hand side of (3.2-2) is approximately zero. The fourth term is identically zero because the gating signal g2 is low during the commutation interval and the 2-winding current remains constant at zero. Only the third term of (3.2-2), i.e. $-L_{ss}pi_1$, contributes to the transistor's collector-to-emitter voltage during commutation of transistor T1. The value of this term was estimated from experimental measurements as three hundred volts. In order to prevent such a large voltage, which would damage the transistor, the Zener diode is used to limit the collector-to-emitter voltage to a value below the break-down voltage. Thus, the upper bound for the Zener voltage, V_z, is the collector-to-emitter break-down voltage, $V_z < V_{ce}^{break}$.

The lower limit for the Zener voltage, $2V_{dc} < V_z$, is needed to prevent the voltage induced in the 1-winding from zenering the diode during the interval T1 is off. During the interval in which T1 is off, the 1-winding current is zero and (3.2-2) simplifies to

$$v_{ce1} = V_{dc} + L_m pi_2 - p\lambda_m \tag{3.2-3}$$

An expression for the time rate of change of 2-winding current, pi_2, can be obtained from (2.4-8) which is repeated here

$$v_2 = r_s i_2 - L_m pi_1 + L_{ss} pi_2 - p\lambda_m \tag{3.2-4}$$

Solving (3.2-4) for pi_2 and substituting into (3.2-3) yields

$$v_{ce1} = V_{dc} + \frac{L_m}{L_{ss}}[v_2 - r_s i_2 + L_m pi_1 + p\lambda_m] - p\lambda_m \tag{3.2-5}$$

Substituting V_{dc} for v_2, setting pi_1 to zero, and collecting terms yields

$$v_{ce1} = (1 + \frac{L_m}{L_{ss}})V_{dc} - \frac{L_m}{L_{ss}} r_s i_2 + (1 - \frac{L_m}{L_{ss}})p\lambda_m \qquad (3.2\text{-}6)$$

This represents the collector-to-emitter voltage of T1 when T2 is on (T1 is off). The ratio of L_m to L_{ss} is the coefficient of coupling between the windings and is nearly unity, so the first factor of the first term is nearly two and the first factor of the last term is nearly zero. Neglecting the voltage drop across the winding resistance, $r_s i_2$,

$$v_{ce1} \cong 2V_{dc} \qquad (3.2\text{-}7)$$

Thus, during the interval that transistor T1 is off, a voltage of approximately twice the dc supply voltage is induced across the parallel combination of transistor T1 and diode D1. The value selected for the Zener voltage, V_z, must be greater than the induced voltage, $2V_{dc}$, in order to prevent the diode from zenering and thereby permitting current to flow in the 1-winding.

3.3 Inverter Switching Logic

The inverter switching logic utilizes a rotor position signal provided by the motor's Hall-effect sensor to generate gating signals (base-drive) for the switching transistors described previously. The use of sensed rotor position to control switching ensures that the requisite synchronism between the brushless dc motor's electrical frequency and rotor speed is maintained. A schematic diagram of the switching logic is shown in Fig. 3.3–1. Two paths of standard and open-collector (o.c.) TTL gates process the rotor position signal into complementary gating signals, g1 and g2. The rotor position signal and

corresponding gating signals for the actual four-pole machine are shown in Fig. 3.3–2.

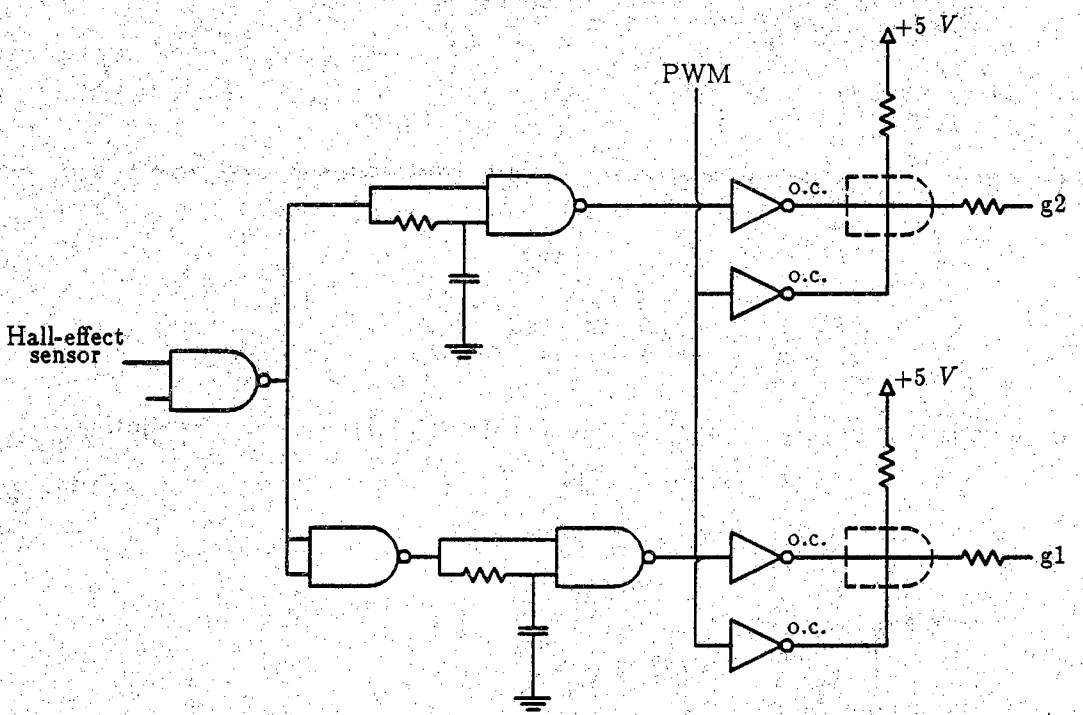

Figure 3.3–1 Schematic diagram of the inverter switching logic.

Signals propagate from left to right in the schematic diagram; the important features of the switching logic will be discussed in a similar order. The output of the motor's Hall-effect sensor is the input to the switching logic. The TTL compatible sensor output feeds one input of the nand-gate shown at the far left-hand side of Fig. 3.3–1. The other nand-gate input is not used. The nand-gate serves merely as a buffer, isolating the motor and inverter electronics and providing sufficient fan-out for the two signal paths. A nand-gate wired as a logic inverter in the lower path results in the gating signal g2

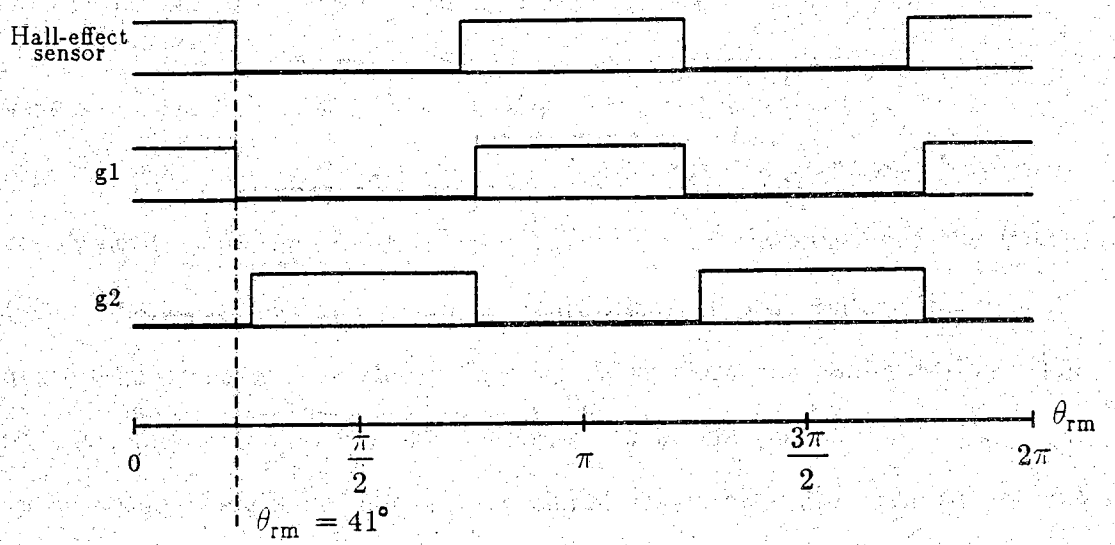

Figure 3.3–2 Plot of the transistor gating signals versus rotor position.

being the complement of gating signal g1, except during commutation. Aside from the additional nand-gate in the lower path, the two paths are identical.

Beyond satisfying the frequency and phase requirements for the gating signals, the switching logic produces small delays (approximately 10 μs) in the low-to-high transitions of the gating signals to allow for commutation. The delay permits commutation of a transistor to be completed before the other transistor is energized. The gating signal transitions are delayed by the combination of an RC network and nand-gate.

The final level of logic provides the base-drive necessary to switch the bipolar transistors. As a convenience, the TTL gates are used to drive the switching transistors directly. This obviates the need for additional transistor networks or darlington transistors. But because standard TTL gates do not source the current required to drive the bipolar transistors into saturation,

open collector TTL gates were used instead. The use of open collector gates also allows the facility for pulse width modulation (PWM) to be incorporated in the switching logic. The so-called "wire-tied and", indicated by a dashed and-gate symbol in Fig. 3.3—1, allows a gating signal to be forced low regardless the state generated by the previous switching logic. An external source provides the PWM signal.

CHAPTER 4
STARTING CHARACTERISTICS

4.1 Introduction

It might be expected that a single-phase brushless dc motor would be unable to accelerate from stall (self-start). The given single-phase brushless dc motor, however, does accelerate from stall with one hundred percent repeatability. In this chapter, the motor's starting characteristics are analyzed in terms of the so-called static electromagnetic and cogging torques. The static electromagnetic torque characteristics for the given motor are derived from information presented in previous chapters. Following this derivation, an empirical approach is used to approximate the motor's cogging torque. Finally, the two torque characteristics are superimposed and used to explain the starting response.

4.2 Static Electromagnetic Torque

In order to accelerate from stall, an initially unexcited motor must develop sufficient electromagnetic torque to overcome torques due to friction, magnetic attraction between stator and rotor members, and any external loads. A problem associated with commutated single-phase motors is that if the rotor

initially rests in certain positions called dead-points, little or no (static) electromagnetic torque is developed. Static electromagnetic torque is the torque developed by the interaction of stator currents with the magnetic field of the rotor permanent magnets when the motor is at or near stall and the stator currents are limited primarily by the stator winding resistance (the back emf is small by comparison). Generally, the static electromagnetic torque for a commutated single-phase motor varies widely with rotor position, including zero or negative torque for some rotor positions.

Using the expression for electromagnetic torque derived in Section 2.4, the inverter gating sequence in Section 3.3, and a scaled plot of measured open-circuit induced voltage (back emf), a plot of the static electromagnetic torque versus rotor position for the given motor will be derived. The expression for electromagnetic torque, T_e, given by (2.4-17) is repeated here for convenience

$$T_e = (i_1 - i_2)\frac{d\lambda_m}{d\theta_r} - \frac{dW_{pm}}{d\theta_r} \qquad (4.2\text{-}1)$$

The second term on the right-hand side of (4.2-1), $-\frac{dW_{pm}}{d\theta_r}$, represents torque related to the magnetic field of the rotor permanent magnets and is independent of the stator currents. This torque will be called the cogging torque, T_{ec}, and is the subject of the next section. The first term on the right-hand side of (4.2-1), $(i_1 - i_2)\frac{d\lambda_m}{d\theta_r}$, represents torque due to the interaction of the stator currents with the magnetic field of the rotor permanent magnets. This torque will be called the dynamic electromagnetic torque and denoted as T_{ed}. The term dynamic is used because, in general, the currents involved in this torque are determined by the stator electrical system dynamics. When the

rotor is at or near stall, however, the electrical system dynamics (described by differential equations) simplify to a static condition (described by algebraic equations). Under the static condition, the stator winding currents will be denoted i_{1o} and i_{2o} and the first term of (4.2-1) will be referred to as the static electromagnetic torque,

$$T_{es} = (i_{1o} - i_{2o})\frac{d\lambda_m}{d\theta_r} \tag{4.2-2}$$

The value of the first factor on the right-hand side of (4.2-2), $(i_{1o} - i_{2o})$, depends upon the rotor position, θ_r, through the gating sequence of the inverter supplying the motor currents (voltages). Plots of the static winding currents versus rotor position appear in Fig. 4.2–1. The plots of i_{1o} and i_{2o} have the same basic form as the gating signals, g1 and g2, shown in Fig. 3.3–2. A minor difference is that a commutation interval is not included for the static currents; the small time delay accounted for by the commutation interval in the gating signals is inconsequential when the rotor is at or near stall. The value of the static stator winding currents, i_{1o} and i_{2o}, is calculated by dividing the dc supply voltage, V_{dc}, by the stator winding resistance, i_{1o} or $i_{2o} = \frac{12\,V}{3.7\,\Omega} = 3.2\,A$. This value is indicated in Fig. 4.2–1. The difference, $i_{1o} - i_{2o}$, is also plotted in Fig. 4.2–1.

A plot of the second factor on the right-hand side of (4.2-2), $\frac{d\lambda_m}{d\theta_r}$, can be obtained from measurements of open-circuit induced voltage (back emf). Using Faraday's law, the open-circuit induced voltage across the 1-winding can be written as

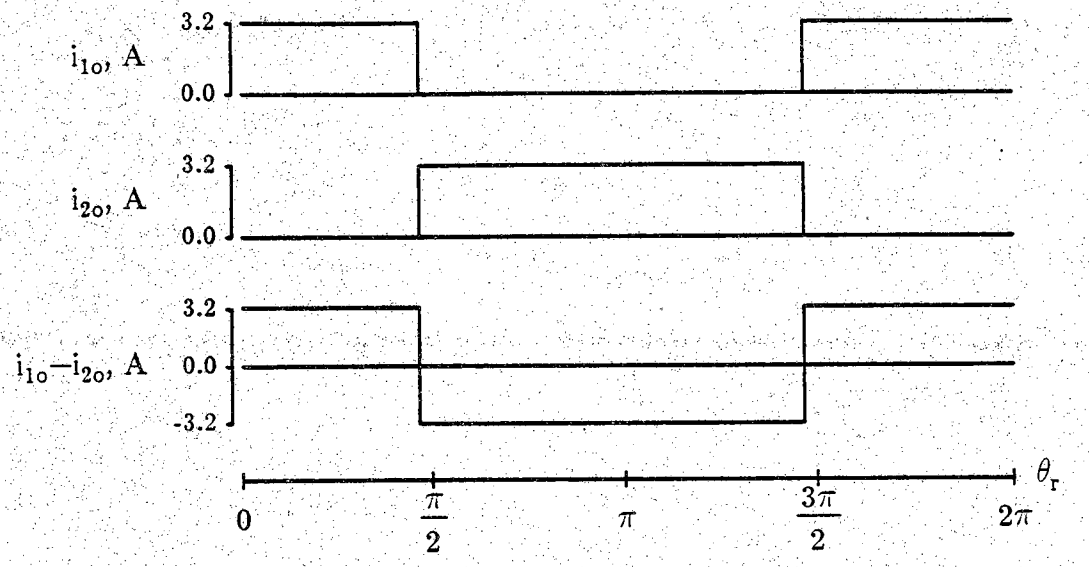

Figure 4.2–1 Plot of the static stator winding currents and their difference.

$$v_1 = \frac{d\lambda_m}{dt} \tag{4.2-3}$$

Applying the chain rule of calculus yields

$$v_1 = \frac{d\lambda_m}{d\theta_r}\frac{d\theta_r}{dt} \tag{4.2-4}$$

Replacing $\frac{d\theta_r}{dt}$ with ω_r yields

$$v_1 = \omega_r \frac{d\lambda_m}{d\theta_r} \tag{4.2-5}$$

Thus, dividing the measured open-circuit voltage, v_1, for a mechanically driven motor by the rotor speed, ω_r, yields $\frac{d\lambda_m}{d\theta_r}$. Because $\frac{d\lambda_m}{d\theta_r}$ represents the back emf when the rotor speed is unity, it will be referred to hereafter as the unitized back emf. The unitized back emf is plotted in Fig. 4.2–2.

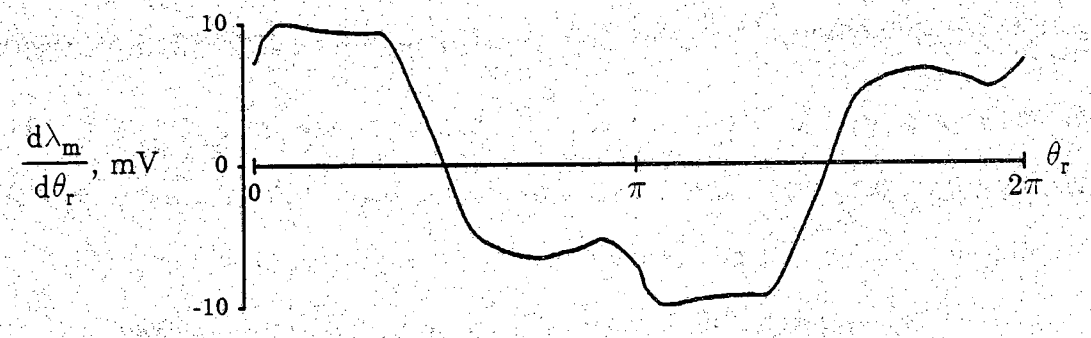

Figure 4.2–2 Plot of the unitized back emf.

Multiplying on a point by point basis, the quantity $i_{1o} - i_{2o}$, plotted in Fig. 4.2–1, by $\frac{d\lambda_m}{d\theta_r}$, plotted in Fig. 4.2–2, yields T_{es}, plotted in Fig. 4.2–3. The plot of T_{es} indicates that when the rotor is stalled, a positive accelerating torque is developed at most rotor positions. In some rotor positions, however, a negative (or flyback) torque results from energizing the motor. The purpose of the cogging torque and detents, discussed in the next section, is to ensure that the rotor position for an initially unexcited motor is in one of the regions where positive static electromagnetic torque is developed.

4.3 Cogging Torque and Detents

The second term on the right-hand side of (4.2-1), $-\frac{dW_{pm}}{d\theta_r}$, represents torque due to the interaction of the magnetic field of the rotor permanent magnets with the stator steel. In particular, it is considered to be a torque

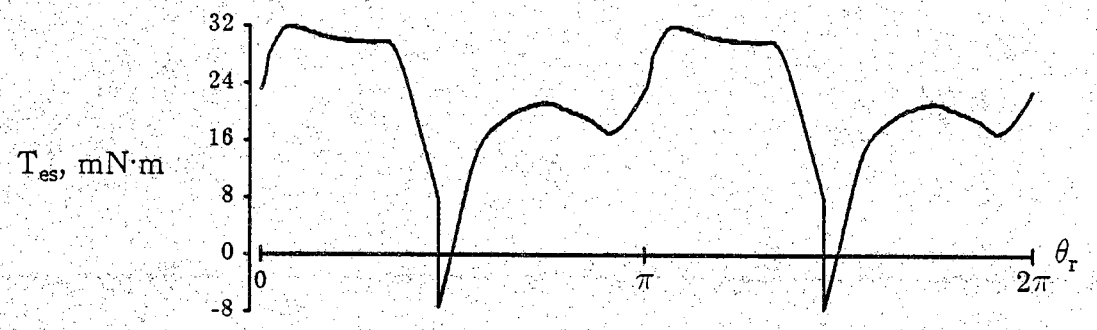

Figure 4.2–3 Plot of the static electromagnetic torque.

which acts to move the rotor (magnets) toward a position at which the stator steel offers a minimum reluctance path. A derivation of the exact form of this term requires advanced analysis. However, an empirical approach is used herein in which the cogging torque is measured at several rotor positions.

The first rotor positions considered are the so-called (stable) detents. These are equally spaced positions for which the rotor has an affinity. The stable detents are the intentional result of the stator asymmetry. At the stable detent positions, the rotor poles cover the raised portions of the stator pole face as depicted in Fig. 4.3–1. Any small disturbance that moves the rotor away from a detent results in a torque which acts to return the rotor to the detent. This implies that at a detent, the cogging torque is zero, $T_{ec} = 0$, and that the slope of the cogging torque characteristic is negative. These features are included in a plot of the cogging torque characteristic in Fig. 4.3–2.

Located midway between the stable detents are unstable detents. If the rotor is moved to an unstable detent, it will have an equal tendency to rotate in the clockwise (cw) or counterclockwise (ccw) direction. However, any small perturbation near an unstable detent will cause the rotor to move away from

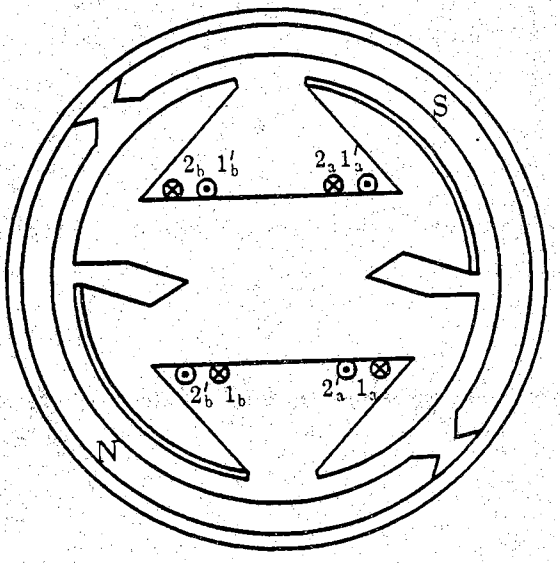

Figure 4.3—1 The rotor positioned at a stable detent.

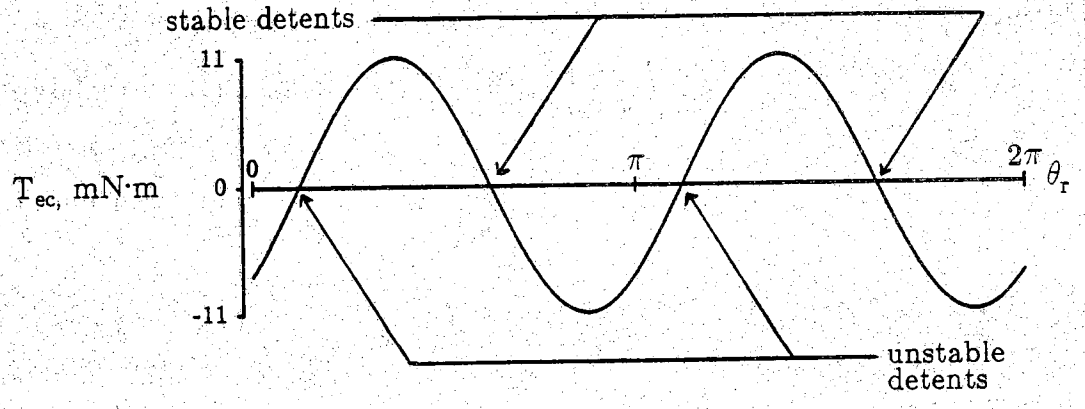

Figure 4.3—2 Plot of the cogging torque.

the unstable detent toward a stable detent. This implies that at an unstable detent, the cogging torque is zero, $T_{ec} = 0$, and the slope of the T_{ec}-characteristic is positive.

Moving counterclockwise (in the direction of increasing θ_r) from a stable detent, the cogging torque decreases to a minimum of $-11\,\text{mN}\cdot\text{m}$ midway between the stable and unstable detents. A maximum cogging torque having approximately the same magnitude occurs midway between the unstable detents and detents. In subsequent discussions, the cogging torque is assumed to be sinusoidal, connecting the zeros and extrema as depicted in Fig. 4.3—2.

4.4 Starting Characteristics

Using the derived static electromagnetic torque curve and the approximate cogging torque curve, the single-phase brushless dc motor's self-starting capability can be explained. It will be assumed that near stall, friction can be neglected and that no external loads are present. Only the static electromagnetic torque and cogging torque are considered. Plots of both torques are superimposed in Fig. 4.4—1.

For an initially unexcited motor, the cogging torque drives the rotor to rest at one of the stable detent positions indicated in Fig. 4.4—1. When the appropriate stator winding is energized, a positive static electromagnetic torque (approximately $18\,\text{mN}\cdot\text{m}$) acts to accelerate the rotor. The rotor moves away from the stable detent in the direction of increasing rotor position (toward the right in Fig. 4.4—1 or counterclockwise in Fig. 4.3—1). As the rotor position increases, the cogging torque acts to return the rotor to the detent position. The positive static electromagnetic torque, however, has greater magnitude and the net torque continues to create a positive acceleration - the rotor position continues to increase. Upon reaching the unstable detent, the cogging torque

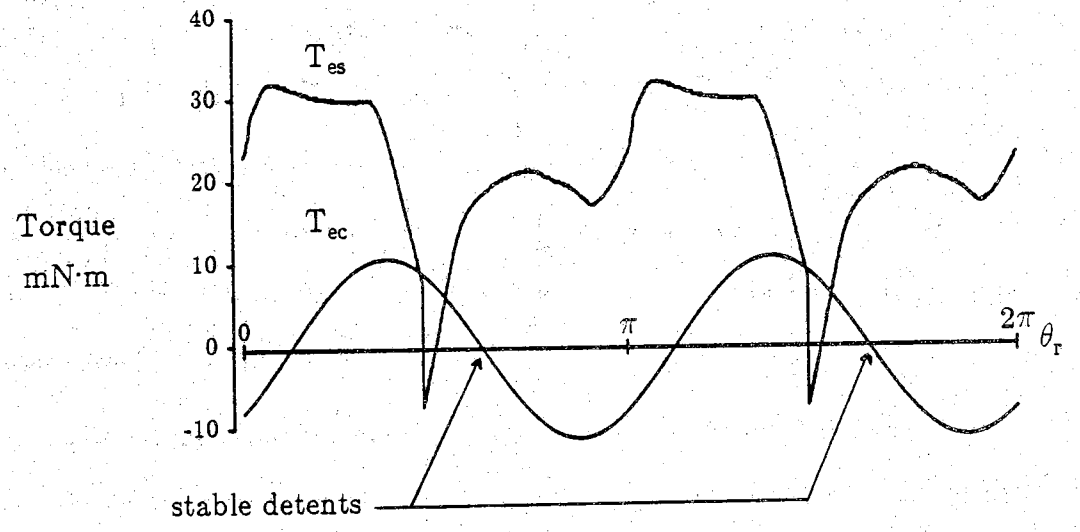

Figure 4.4—1 Superimposed plots of the static electromagnetic torque and the cogging torque.

becomes positive and contributes to positive rotor acceleration. The positive cogging torque combined with rotor inertia prevent the negative static electromagnetic torque immediately following commutation from bringing the motor back to stall.

The static electromagnetic torque continues to accelerate the rotor until the back emf created by the rotating magnetic field of the permanent magnets begins to appreciably reduce the stator currents at rotor speeds around 100 rad/s. For $\omega_r > 100$ rad/s, the accelerating torque is attributable to the dynamic electromagnetic torque, rather than the static electromagnetic torque. Also, at these speeds, the instantaneous pulsations in the cogging torque become less significant because of rotor inertia. Under the influence of the dynamic electromagnetic torque, the motor continues to accelerate until the

increasing back emf decreases the winding currents (electromagnetic torque) to a level at which the electromagnetic torque equals the torque due to windage and friction.

A load torque can be accounted for during starting by decreasing the net accelerating torque. At higher speeds, the dynamic electromagnetic torque must counter both the load torque and torque due to friction and windage.

CHAPTER 5
COMPUTER SIMULATION

5.1 Introduction

A computer simulation of the single-phase brushless dc motor was developed to investigate its steady-state and dynamic performance. In this chapter, the mathematical model derived in Chapter 2 is expressed in a form amenable to computer simulation. After developing an appropriate computer model for the synchronous machine, the implementation of the computer simulation is described. Since the brushless dc motor is supplied by a dc-to-ac inverter, the simulation also requires a mathematical model of the inverter. Two different models of the inverter are developed and investigated. Using each model, the steady-state and dynamic characteristics of the motor, operating at rated speed and without mechanical load are established. Experimentally measured voltage and current waveforms serve as a benchmark for the simulation results and indicate that the computer modeling of the motor is quite accurate.

5.2 A State Model for the Machine

In order to facilitate development of a computer simulation, the mathematical model derived in Section 2.4 was rewritten in the following state-model form [4]

$$\dot{\mathbf{x}} = \mathbf{f}(\mathbf{x}(t),\mathbf{u}(t),t) \tag{5.2-1}$$

where $\mathbf{x}(t)$ is a vector of state variables, $\mathbf{u}(t)$ is a vector of input variables, and $\mathbf{f}(\cdot,\cdot,\cdot)$ is a vector-valued function. In this section, the state variables are identified and the derivation of the state model is presented.

The computer simulation is based upon the equations describing the dynamics of the electrical and mechanical systems derived in Section 2.4 and repeated here for convenience.

$$v_1 = r_s i_1 + L_{ss} p i_1 - L_m p i_2 + p\lambda_m \tag{5.2-2}$$

$$v_2 = r_s i_2 - L_m p i_1 + L_{ss} p i_2 - p\lambda_m \tag{5.2-3}$$

$$T_e = Jp\omega_r + B\omega_r + T_L \tag{5.2-4}$$

An approximate expression for the electromagnetic torque is obtained from (2.4-17) by omitting the term associated with the cogging torque, T_{ec}. In particular,

$$T_e = (i_1 - i_2)\frac{d\lambda_m}{d\theta_r} \tag{5.2-5}$$

This omission is reasonable because the cogging torque has zero average-value over one revolution and, even at low speeds, the effect of the cogging torque pulsations on rotor speed is filtered by the rotor's relatively large moment of inertia.

Four state variables are needed to describe the combined electrical and mechanical system. The stator winding currents, i_1 and i_2, are selected as state variables. The rotor speed, ω_r, is also a state variable. Because the machine is a synchronous machine, and in particular a brushless dc motor wherein inverter switching is related to rotor position, it is necessary to include the rotor position, θ_r, as a state variable. The resulting vector of state variables is

$$\mathbf{x} = [\, i_1 \;\; i_2 \;\; \omega_r \;\; \theta_r \,]^T \tag{5.2-6}$$

where the superscript T denotes transpose.

The process of converting (5.2-2) to (5.2-4) to state-model form involves solving each one of the equations for the time rate of change of one of the state variables. In order to simplify manipulation of the voltage equations, (5.2-2) and (5.2-3) are put in the form of a matrix-vector equation

$$\begin{bmatrix} v_1 \\ v_2 \end{bmatrix} = \begin{bmatrix} r_s i_1 \\ r_s i_2 \end{bmatrix} + \begin{bmatrix} L_{ss} & -L_m \\ -L_m & L_{ss} \end{bmatrix} \begin{bmatrix} pi_1 \\ pi_2 \end{bmatrix} + \begin{bmatrix} p\lambda_m \\ -p\lambda_m \end{bmatrix} \tag{5.2-7}$$

Solving for the vector containing pi_1 and pi_2 by collecting all other terms and pre-multiplying by the inverse of the inductance matrix yields

$$\begin{bmatrix} pi_1 \\ pi_2 \end{bmatrix} = \frac{1}{L_{ss}^2 - L_m^2} \begin{bmatrix} L_{ss} & L_m \\ L_m & L_{ss} \end{bmatrix} \begin{bmatrix} v_1 - r_s i_1 - p\lambda_m \\ v_2 - r_s i_2 + p\lambda_m \end{bmatrix} \tag{5.2-8}$$

The coefficient of coupling, k, will be defined as the ratio of the magnetizing inductance, L_m, to the self-inductance, L_{ss}, and is used in rewriting (5.2-8) as

$$\begin{bmatrix} pi_1 \\ pi_2 \end{bmatrix} = \frac{1}{L_{ss}(1 - k^2)} \begin{bmatrix} 1 & k \\ k & 1 \end{bmatrix} \begin{bmatrix} v_1 - r_s i_1 - p\lambda_m \\ v_2 - r_s i_2 + p\lambda_m \end{bmatrix} \tag{5.2-9}$$

This vector equation may be expressed as two scalar equations, one for each of

the two stator winding currents. In addition, $p\lambda_m$ can be expressed as $\omega_r \frac{d\lambda_m}{d\theta_r}$. Thus,

$$pi_1 = \frac{1}{L_{ss}(1-k^2)}\left[(v_1 - r_s i_1) + k(v_2 - r_s i_2) - (1-k)\omega_r \frac{d\lambda_m}{d\theta_r}\right] \qquad (5.2\text{-}10)$$

$$pi_2 = \frac{1}{L_{ss}(1-k^2)}\left[k(v_1 - r_s i_1) + (v_2 - r_s i_2) + (1-k)\omega_r \frac{d\lambda_m}{d\theta_r}\right] \qquad (5.2\text{-}11)$$

The equation for the mechanical dynamics (5.2-4) provides an expression for the time rate of change of rotor velocity,

$$p\omega_r = \frac{1}{J}(T_e - B\omega_r - T_L) \qquad (5.2\text{-}12)$$

An expression for the time rate of change of rotor position is obtained by equating $p\theta_r$ with ω_r,

$$p\theta_r = \omega_r \qquad (5.2\text{-}13)$$

In (5.2-10) to (5.2-12) the applied stator voltages, v_1 and v_2, and the load torque, T_L represent inputs variables. The vector of input variables may be written

$$\mathbf{u} = [\, v_1 \;\; v_2 \;\; T_L \,]^T \qquad (5.2\text{-}14)$$

Equations (5.2-10) to (5.2-13) along with the state and input vectors defined by (5.2-6) and (5.2-14), respectively, comprise a state-model description of the electromechanical dynamics of the single-phase brushless dc motor.

5.3 Computer Simulation

The digital computer simulation of the motor uses an Euler-predictor, trapezoidal-corrector algorithm with variable length time steps [5] to integrate the state equations, (5.2-10) to (5.2-13). In order to calculate the rate of change of the electrical state variables using (5.2-10) and (5.2-11), the value of the input variables v_1 and v_2 along with the unitized back emf, $\frac{d\lambda_m}{d\theta_r}$, must be determined at each time step.

The applied stator winding voltages, v_1 and v_2, are calculated using a mathematical model of the dc-to-ac inverter which drives the brushless dc motor. For convenience, the schematic diagram of the inverter, described in Chapter 3, is redrawn with each inverter leg connected to a terminal of the stator winding equivalent circuit in Fig. 5.3—1. Two different mathematical models of this inverter were developed for the computer simulation. The inverter model which will be described in the next section uses idealized current-voltage (I-V) characteristics to model the inverter's transistors and diodes. In Section 5.5, a so-called functional representation of the inverter is presented.

In both models, four intervals of inverter operation (combinations of transistor conduction states) are considered. In the simulation, the procedure for determining the appropriate interval of inverter operation emulates the function of the switching logic in the actual inverter. Accordingly, the criteria used to determine the conduction interval are: (1) the rotor position and (2) the elapsed time since the last change of interval. The commutation angle, θ_c, is a simulation parameter that determines the rotor position at which

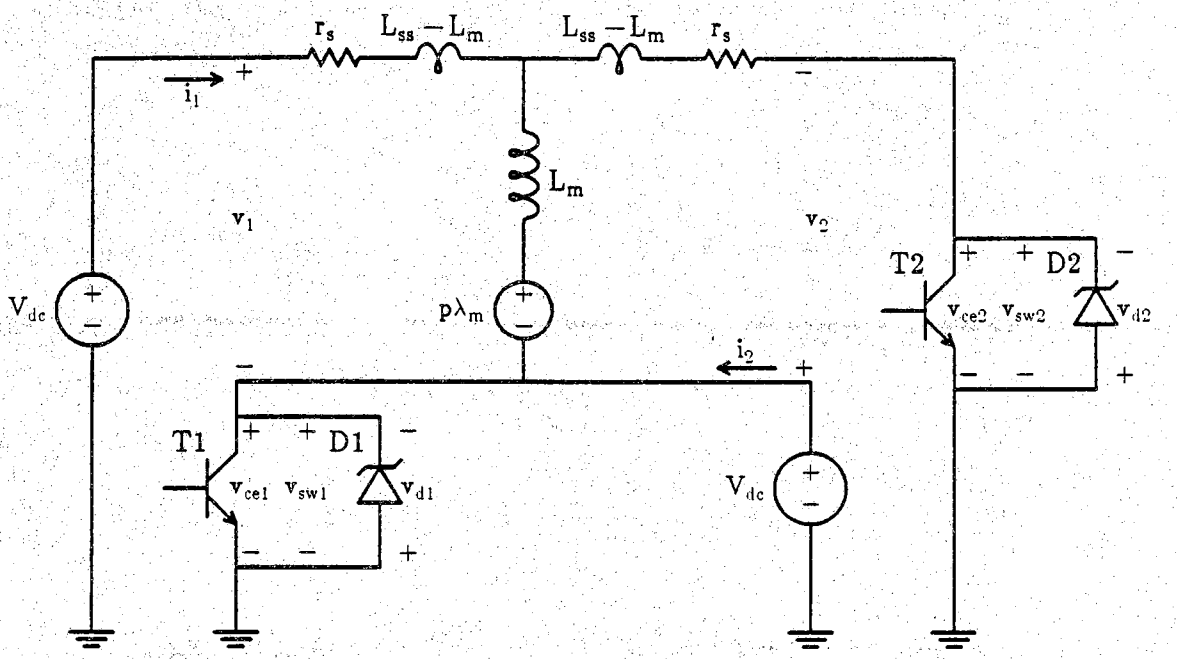

Figure 5.3—1 Schematic diagram of the winding equivalent circuit and dc-to-ac inverter.

commutation from transistor T1 to transistor T2 begins. The normal value for the commutation angle, $\theta_c = 82^\circ$, was obtained experimentally by noting the difference in rotor position between transitions in the Hall-effect sensor output and the zero-crossings of the open-circuit voltage for a mechanically driven motor. Generally, for rotor positions less than the commutation angle (and greater than the commutation angle plus or minus 180°) the simulation considers transistor T1 to be on and T2 to be off. The interval when T1 is on and T2 is off will be referred to as T1ON. At the instant the rotor passes through the commutation angle, the time, t, is stored as the commutation time, t_c, and transistor T1 is subsequently considered to be commutating off while T2 remains off. This interval is the so-called commutation interval of

transistor T1 and will be referred to as T1COMM. The T1COMM interval lasts for a fixed-time commutation delay, t_{delay}. The value used for the commutation delay is 10 μs, which was the value measured for the actual inverter. At each time step, the elapsed time since passing through the commutation angle is compared to the commutation delay. When the elapsed time is greater than the commutation delay, the simulation considers the commutation of T1 to be complete and T2 to be on. This interval will be called T2ON. An interval T2COMM, which is similar to T1COMM, begins when the rotor position passes through the commutation angle plus 180°. The transistor conduction states and bounds of the four intervals are summarized in Table 5.3–1.

The unitized back emf, $\frac{d\lambda_m}{d\theta_r}$, appearing in the state model equations (5.2-10) and (5.2-11) and the torque equation (5.2-5), is a function only of rotor position and is determined using a simple data look-up procedure. Data for the unitized back emf was digitally recorded and is loaded into an array prior to entering the integration loop. At the start of each predictor and corrector iteration, the value of the rotor position, θ_r, is used to calculate an array index which, in turn, is used to access the value of $\frac{d\lambda_m}{d\theta_r}$ which corresponds to that rotor position.

The procedure for updating the state variables at each time step in the simulation is briefly outlined as follows. At the start of each time step, the inverter interval is determined based upon the rotor position at the end of the previous time step. Next, the unitized back emf and applied stator voltages for the predictor iteration are determined. All calculations during the predictor

Table 5.3—1 The four intervals of inverter operation.

Interval	Conduction State		Bounds
	T1	T2	
T1ON	on	off	$(\theta_r < \theta_c)$ or $(\theta_r \geqq \theta_c + 180°)$ and $t - t_c > t_{delay}$
T1COMM	commutating off	off	$\theta_c \leqq \theta_r < \theta_c + 180°$ and $t - t_c < t_{delay}$
T2ON	off	on	$\theta_c < \theta_r \leqq \theta_c + 180°$ and $t - t_c > t_{delay}$
T2COMM	off	commutating off	$(\theta_r < \theta_c)$ or $(\theta_r \geqq \theta_c + 180°)$ and $t - t_c < t_{delay}$

iteration use the value of the state variables at the end of the previous time step. The electromagnetic torque is calculated from the winding currents and the unitized back emf. Then, the rate of change of all state variables is calculated and a predicted value for each state variable is determined. Using these predicted values, the unitized back emf and applied voltages are recalculated for the corrector iteration. The calculations of torque and rates of change are repeated. Finally, the updated value of each state variable is determined using the average of its rates of change calculated in the predictor and corrector iterations.

5.4 An I-V Characteristic Model of the Inverter

The first method developed for calculating the applied stator voltages utilizes piecewise-linear I-V characteristics to calculate the voltage across the inverter switching elements (transistors and diodes). In this section, the I-V characteristics (circuit models) for the transistors and diodes are presented. The use of these models in the computer simulation is then discussed.

Equations in the following derivation are written for transistor T1 and diode D1, but are equally valid, with an appropriate change of subscripts, for transistor T2 and diode D2. A switch voltage, v_{sw1}, is indicated in Fig. 5.3–1 as the voltage across the parallel combination of transistor T1 and diode D1. Expressions for the transistor voltage, v_{ce1}, and diode voltage, v_{d1}, will be related to the switch voltage, v_{sw1}, which, in turn, is related to the applied stator winding voltage, v_1, by the equation

$$v_1 = V_{dc} - v_{sw1} \tag{5.4-1}$$

When a transistor is on (operated in saturation), it is modeled as a small resistor connected between the collector and emitter terminals [6]. In this case, the switch voltage, v_{sw1}, which equals the transistor's collector-to-emitter voltage, is given by

$$v_{sw1} = v_{ce1} = r_{sat} i_1 \tag{5.4-2}$$

where r_{sat} is the transistor's collector-to-emitter saturation resistance and is approximately 0.5 Ω. Because the switch voltage is also across the parallel diode, it is restricted to values between the Zener and forward conduction voltages of the diode as described in the subsequent discussion.

When a transistor is off (operated in cutoff) or being commutated off, the transistor is considered to be an open-circuit and the I-V characteristic of the parallel diode determines the switch voltage. The diode I-V characteristic used for the simulation is depicted in Fig. 5.4—1 with the slopes exaggerated for clarity. In the diode's reverse bias region of operation, between the negative Zener voltage, $-V_z$, and the forward conduction voltage, V_b, the characteristic has a positive slope of $\frac{1}{r_{rev}}$, and the diode voltage is related to the diode (negative 1-winding) current by

$$v_{d1} = -r_{rev} i_1 \qquad \text{for} \quad -V_z < v_{d1} < V_b \tag{5.4-4}$$

Diode voltages calculated using (5.4-4) which are less than the negative Zener voltage are clamped at $v_{d1} = -V_z$, but generally this is not necessary because the value selected for the Zener voltage prevents zenering except during commutation. Voltages above the forward conduction voltage are fixed at the forward conduction voltage, $v_{d1} = V_b$. From Fig. 5.3—1, the switch voltage equals the opposite of the diode voltage, $v_{sw1} = -v_{d1}$.

The model used for each transistor-diode pair in a given interval follows directly from the conduction states listed in Table 5.3—1. For example, during T1ON, transistor T1 is on and modeled by a transistor saturation resistance while T2 is off and modeled by a diode reverse leakage resistance. By symmetry, the models are exchanged during T2ON. During the commutation intervals, T1COMM and T2COMM, both transistor-diode pairs are modeled by the diode I-V characteristic depicted in Fig. 5.4—1. Models for the switching elements are summarized in Table 5.4—1. After calculating the switch voltages, the applied stator voltages are calculated by subtracting the switch

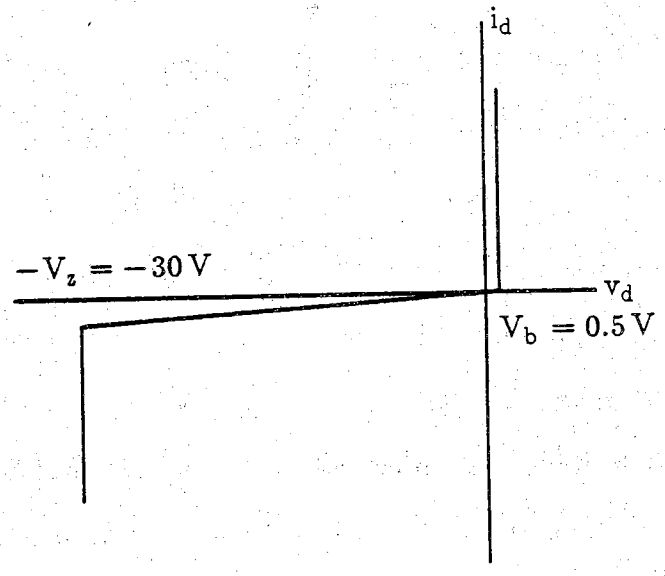

Figure 5.4—1 Diode I-V characteristic used in the computer simulation.

voltages from the dc supply voltage.

Although the previous I-V characteristics of the transistors and diodes are easily implemented in a computer program, the resulting simulation requires extremely small time steps. The need for a small time step can be explained by considering the eigenvalues associated with the circuit shown Fig. 5.4—2. This circuit, for the situation when transistor T1 is on and T2 is off (T1ON), is a special case of the equivalent circuit in Fig. 5.3—1 and has a resistor ($r_{rev} = 2\ k\Omega$) replacing the reverse biased diode D2. The circuit eigenvalue with largest modulus is on the order of 10^7, indicating that simulation time steps should be on the order 10^{-7} s. In fact, by trial-and-error, 2.0×10^{-7} s was found to the largest time step that did not result in a numerical instability using the given predictor-corrector algorithm. Although larger time steps are possible by decreasing the value of r_{rev}, this has the adverse effect of permitting

Table 5.4–1 The I-V characteristic model for the switch voltages in each interval of inverter operation.

Interval	Switch Voltage	
	v_{sw1}	v_{sw2}
T1ON	$v_{ce1} = r_{sat} i_1$ if $r_{sat} i_1 > -V_b$ $v_{ce1} = -V_b$ if $r_{sat} i_1 \leqq -V_b$	$-v_{d2} = r_{rev} i_2$ if $r_{rev} i_2 < V_z$ $-v_{d2} = V_z$ if $r_{rev} i_2 \geqq V_z$
T1COMM	$-v_{d1} = r_{rev} i_1$ if $r_{rev} i_1 < V_z$ $-v_{d1} = V_z$ if $r_{rev} i_1 \geqq V_z$	$-v_{d2} = r_{rev} i_2$ if $r_{rev} i_2 > -V_b$ $-v_{d2} = -V_b$ if $r_{rev} i_2 \leqq -V_b$
T2ON	$-v_{d1} = r_{rev} i_1$ if $r_{rev} i_1 < V_z$ $-v_{d1} = V_z$ if $r_{rev} i_1 \geqq V_z$	$v_{ce2} = r_{sat} i_2$ if $r_{sat} i_2 > -V_b$ $v_{ce2} = -V_b$ if $r_{sat} i_2 \leqq -V_b$
T2COMM	$-v_{d1} = r_{rev} i_1$ if $r_{rev} i_1 > -V_b$ $-v_{d1} = -V_b$ if $r_{rev} i_1 \leqq -V_b$	$-v_{d2} = r_{rev} i_2$ if $r_{rev} i_2 < V_z$ $-v_{d2} = V_z$ if $r_{rev} i_2 \geqq V_z$

a larger leakage current in the winding which, for practical purposes should be zero. Decreasing the value of the coupling coefficient, k, also permits a larger time step, but alters the nature of the electrodynamics. A second approach for modeling the inverter is developed in the next section.

Operation of the actual motor-inverter system provided a benchmark for the simulation. Instantaneous winding currents and voltages for a motor operating without external load, $T_L = 0$, and at a (mechanical) speed of 3600 rpm (377 rad/s) were recorded experimentally. The dc supply voltage required to maintain a no-load speed of 3600 rpm was determined through trial-and-error as 6.3 V. Because the given motor is a four pole device, the mechanical speed of 3600 rpm corresponds to an electrical angular frequency of 754 rad/s. Thus, the simulation was performed with $\omega_r = 754$ rad/s. The dc

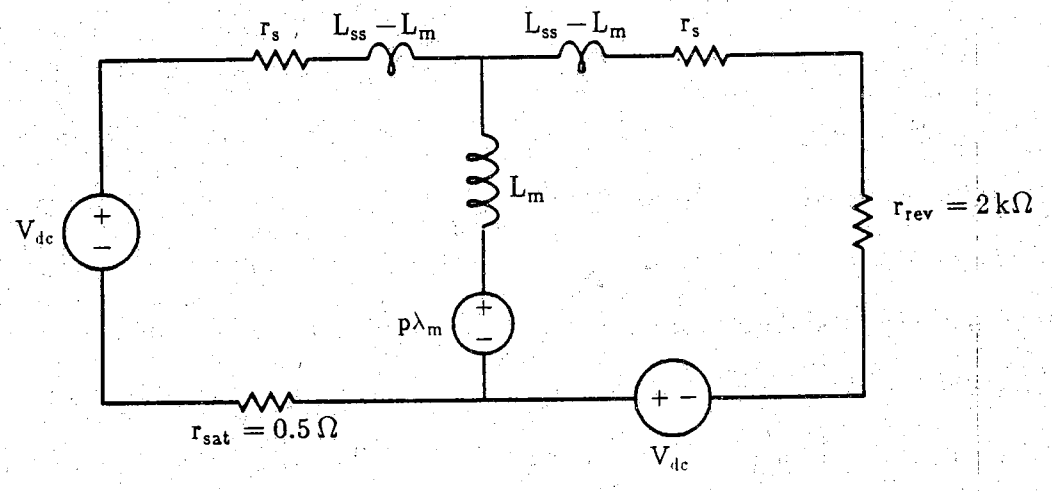

Figure 5.4—2 Schematic diagram of the equivalent circuit for situation when T1 is on and T2 is off.

supply voltage used in the simulation was the same as for the actual motor-inverter. In particular, $V_{dc} = 6.3\,V$. Traces of the 1-winding current and voltage from the simulation are shown along with the experimentally recorded traces in Fig. 5.4—3. The simulation results compare well with the measured waveforms. A more complete set of traces in Fig. 5.4—4 includes the 2-winding current and voltage, as well as the electromagnetic torque, T_e, and the (back) emf.

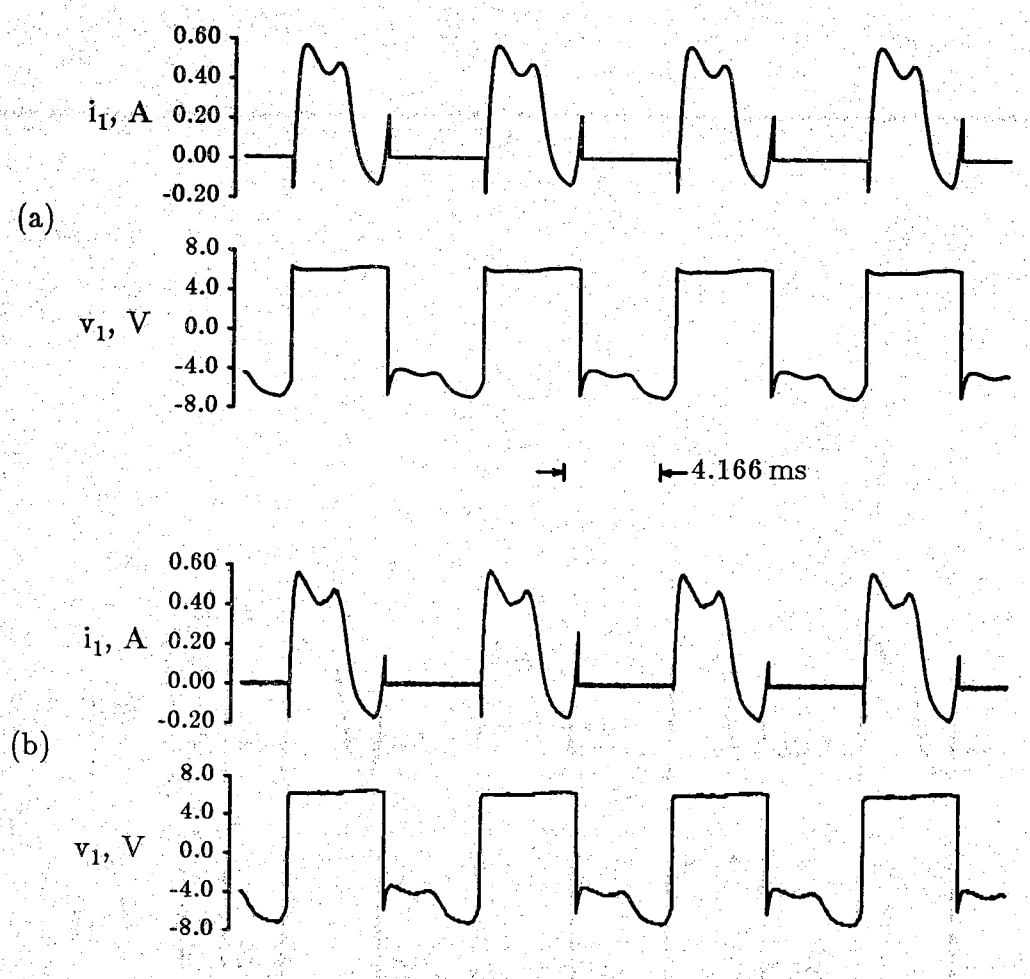

Figure 5.4—3 Comparison of traces from (a) simulation using I-V characteristics and (b) experimental measurement, for a motor operating at $\omega_r = 754$ rad/s and $T_L = 0$.

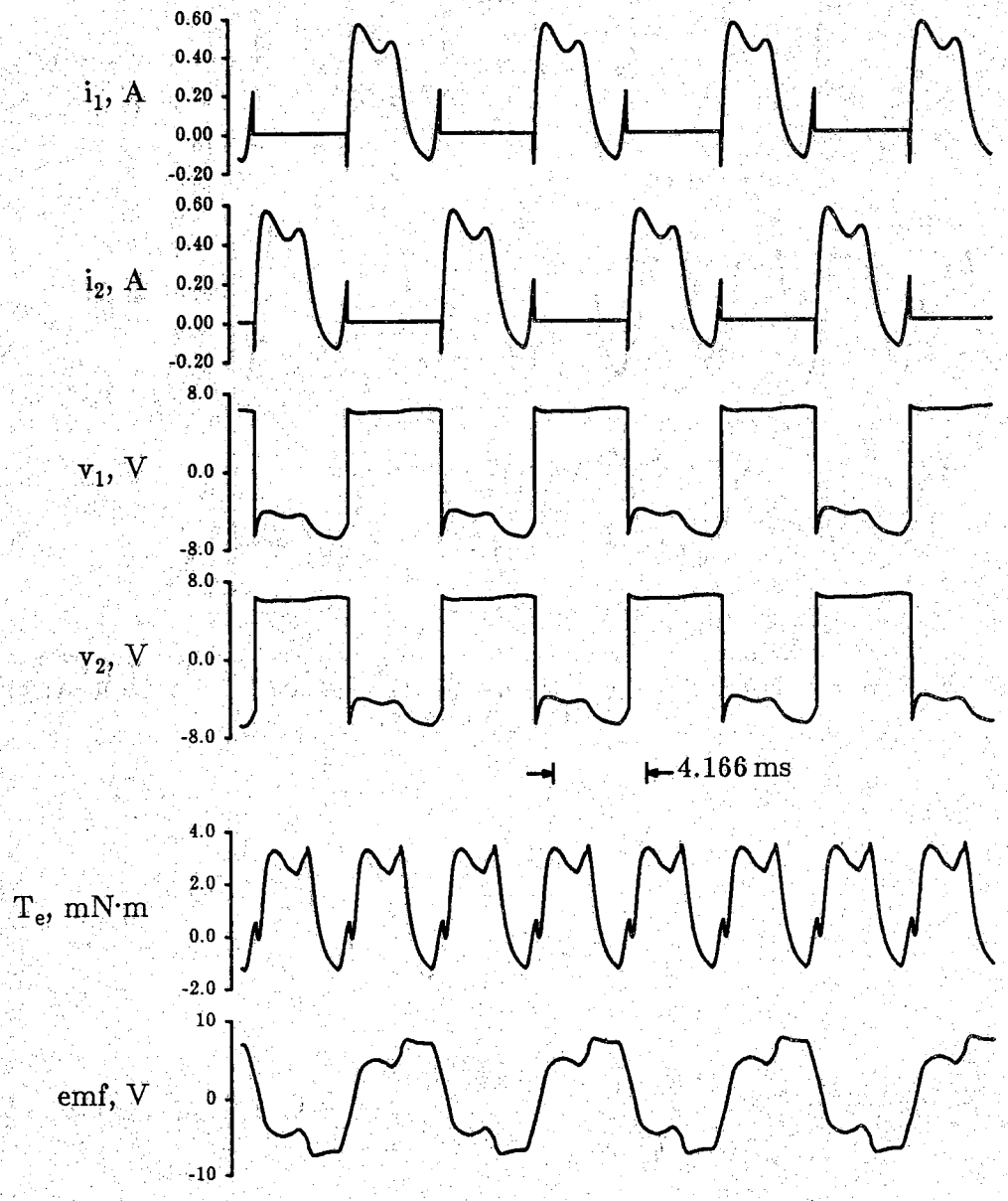

Figure 5.4—4 I-V characteristic simulation results for motor operating at $\omega_r = 754$ rad/s and $T_L = 0$.

5.5 A Functional Representation of the Inverter

In the so-called functional representation of the inverter, the switch voltages, v_{sw1} and v_{sw2}, are calculated at each time step using relationships derived from the voltage equations (5.2-2) and (5.2-3). In particular, modeling of the inverter's switching elements involves calculating the open-circuit voltage which should appear across a transistor-diode pair whenever the transistor is not on. By setting the switch voltage to this calculated open-circuit value and determining the corresponding applied stator voltage, the appropriate winding current is maintained at or driven toward a value corresponding to an open-circuit condition.

The schematic diagram of the winding equivalent circuit and inverter shown in Fig. 5.3—1 will be considered again. In the following derivations, the voltages across transistor T1 and diode D1 during each of the simulation intervals are considered, but in order to simplify references, some of the corresponding equations for transistor T2 and diode D2 are given without derivation.

In the functional model, the voltage applied to the stator winding whose transistor is on must be determined before the switch voltage of the transistor which is off can be calculated. When a transistor is on (operated in saturation), as during the interval T1ON, the transistor is modeled as a voltage source connected between the collector and emitter terminals. In this case, the switch voltage and transistor voltage are given by

$$v_{sw1} = v_{ce1} = V_{ce}^{sat} \tag{5.5-1}$$

Likewise, during T2ON,

$$v_{sw2} = v_{ce2} = V_{ce}^{sat} \tag{5.5-2}$$

where V_{ce}^{sat} is the transistor collector-to-emitter saturation voltage and is approximately 0.25 V. As with the I-V characteristic model, (5.4-1) is used to calculate the applied stator winding voltage from the switch voltage.

Central to the functional representation of the inverter is the relationship between the electric system dynamics and the switch voltage for the transistor which is not on. The diode I-V characteristic places constraints on the switch voltage, and it is convenient to write expressions for the diode voltage rather than for the negative switch voltage. The voltage across diode D1 is obtained from Kirchoff's voltage law applied to the loop containing diode D1, the 1-winding, and the dc voltage supply, i.e.

$$v_{d1} = v_1 - V_{dc} \tag{5.5-3}$$

Substituting (5.2-2) for v_1 yields

$$v_{d1} = r_s i_1 + L_{ss} p i_1 - L_m p i_2 + p\lambda_m - V_{dc} \tag{5.5-4}$$

Solving (5.2-3) for pi_2 and substituting into (5.5-4) yields

$$v_{d1} = r_s i_1 + L_{ss} p i_1 - \frac{L_m}{L_{ss}}[v_2 - r i_2 + L_m p i_1 + p\lambda_m] + p\lambda_m - V_{dc} \tag{5.5-5}$$

Collecting terms and using the coupling coefficient, k, to replace $\frac{L_m}{L_{ss}}$ and $\omega_r \frac{d\lambda_m}{d\theta_r}$ to replace $p\lambda_m$ yields

$$v_{d1} = r_s i_1 + (1 - k^2) L_{ss} p i_1 - k(v_2 - r_s i_2) + (1 - k)\omega_r \frac{d\lambda_m}{d\theta_r} - V_{dc} \tag{5.5-6}$$

Similarly, for diode D2,

$$v_{d2} = r_s i_2 + (1 - k^2) L_{ss} p i_2 - k(v_1 - r_s i_1) - (1 - k)\omega_r \frac{d\lambda_m}{d\theta_r} - V_{dc} \qquad (5.5\text{-}7)$$

Constraints on the diode voltage, v_{d1}, expressed in (5.5-6) result from the device's physical characteristics. In particular, the diode voltage must remain greater than the negative Zener voltage and below the forward conduction voltage, $-V_z < v_{d1} < V_b$. Equation (5.5-6) represents a general expression for the voltage developed across diode D1 due to the electrical dynamics whenever transistor T1 is off or being commutated off. Specific simplifications of (5.5-6) are made when considering each of the intervals T2ON, T2COMM, and T1COMM.

When transistor T1 is off and T2 is on, namely the interval T2ON, the function of T1 and D1 is to prevent current from flowing in the 1-winding, i.e. open-circuit the 1-winding. In this case, i_1 and pi_1 are zero and (5.5-6) may be simplified to

$$v_{d1} = -k(v_2 - r_s i_2) + (1 - k)\omega_r \frac{d\lambda_m}{d\theta_r} - V_{dc} \qquad (5.5\text{-}8)$$

Likewise, during interval T1ON when T2 is off (5.5-7) reduces to

$$v_{d2} = -k(v_1 - r_s i_1) - (1 - k)\omega_r \frac{d\lambda_m}{d\theta_r} - V_{dc} \qquad (5.5\text{-}9)$$

Before evaluating (5.5-8), the 2-winding voltage, v_2, is determined using (5.5-2) and the relationship $v_2 = V_{dc} - v_{sw2}$. The other expressions on the right-hand side of (5.5-8) are readily established from simulation values. By applying the stator voltage corresponding to the open-circuit diode voltage calculated with (5.5-6), the value of the 1-winding current is held at zero throughout the interval T2ON. A different equation, however, must be used to calculate the

stator voltage necessary to drive the 1-winding current from a non-zero value toward zero, i.e. commutate off transistor T1.

While transistor T1 is being commutated off (interval T1COMM), neither the 1-winding current nor its time rate of change are zero. Thus, all terms on the right-hand side of (5.5-6) contribute to the diode voltage, v_{d1}, The differentiation of the state variable i_1 in the second term of (5.5-6), however, makes use of this equation, as written, undesirable. Instead, an algebraic relationship between the diode voltage and a predicted value for the 1-winding current at the end of the time step will be derived from (5.5-6) by solving (5.5-6) as a differential equation. Using the derived algebraic relationship, the diode voltage which would drive the 1-winding current to zero at the end of the time step is calculated. In order to avoid carrying complicated expressions through the derivation of the new expression for v_{d1}, new variables, L_c and v_c, are defined as

$$L_c = (1 - k^2)L_{ss} \tag{5.5-10}$$

$$v_c = V_{dc} + k(v_2 - r_s i_2) - (1 - k)\omega_r \frac{d\lambda_m}{d\theta_r} \tag{5.5-11}$$

All expressions on the right-hand side of (5.5-11) except v_2 are readily established from simulation values at each time step. However, as T1 is being commutated off, the 1-winding current rapidly decreases to zero and a positive voltage is induced in the 2-winding. This induced voltage forward biases diode D2 whereupon $v_2 = V_b$ during this commutation interval. Given v_2, v_c is readily calculated from (5.5-11). The value of v_c obtained from (5.5-11) is assumed constant throughout the time step. Using (5.5-10) and (5.5-11), (5.5-

6) may be rewritten as

$$pi_1 + \frac{r_s}{L_c} i_1 = \frac{1}{L_c}(v_c + v_{d1}) \tag{5.5-12}$$

This is a linear, first-order, inhomogeneous differential equation which is time-invariant over a time step and can be solved in closed form. It is applicable throughout the interval T1COMM. At the start of each time step during T1COMM, the value of the 1-winding current calculated during the previous time step serves as the initial condition $i_1(t_0)$ for (5.5-12). The solution to (5.5-12) with the given initial condition and assuming v_{d1} is constant is

$$i_1(t-t_0) = i_1(t_0)e^{-\frac{r_s}{L_c}(t-t_0)} + \frac{1}{r_s}(v_c + v_{d1})\left(1 - e^{-\frac{r_s}{L_c}(t-t_0)}\right) \tag{5.5-13}$$

Evaluating (5.5-13) at the end of the time step, whose length is h, yields

$$i_1(h) = i_1(t_0)e^{-\frac{r_s}{L_c}h} + \frac{1}{r_s}(v_c + v_{d1})\left(1 - e^{-\frac{r_s}{L_c}h}\right) \tag{5.5-14}$$

Thus, the value of the 1-winding current at the end of a time step can be predicted using (5.5-14). Because the purpose of the diode during commutation is to drive the 1-winding current toward zero, v_{d1} should be calculated so that $i_1(h) = 0$. Setting $i_1(h) = 0$ in (5.5-14) and solving for v_{d1} yields

$$v_{d1} = r_s i_1(t_0) \frac{e^{-r_s h/L_c}}{1 - e^{-r_s h/L_c}} - v_c \tag{5.5-15}$$

Thus during T1COMM, the value of the diode voltage, v_{d1}, which, when applied over the time step h, will drive the 1-winding current to zero is

calculated using (5.5-15). If the calculated v_{d1} is less than $-V_z$, v_{d1} is set to $-V_z$ to take into account zenering.

The applied voltages during the remaining interval, T2COMM, are calculated in the same manner as during T1COMM. The sequence of calculations during all the intervals of inverter operation are summarized in Table 5.5—1.

The use of the functional representation of the inverter permits much longer time steps than the I-V characteristic model. During the intervals T1ON and T2ON, the time step can be as large as $h = 500\,\mu s$, an improvement of 250-fold. Eigenvalue analysis of the winding equivalent circuit with one terminal open circuited (the effect of the functional representation) indicates even longer time steps are possible, but further improvements are limited by the higher space harmonics of the unitized back emf. During the intervals T1COMM and T2COMM, it is necessary to reduce the time step to $5\,\mu s$ in order to accurately model the zenering of the inverter diodes.

Traces of the 1-winding current and voltage from a simulation at $\omega_r = 754$ rad/s and $T_L = 0$ are shown along with expermentally recorded traces in Fig. 5.5—1. A more complete set of traces in Fig. 5.5—2 includes the 2-winding current and voltage as well as the electromagnetic torque, T_e, and the (back) emf.

Table 5.5–1 Sequence of calculations during each interval of inverter operation.

Interval	Sequence of calculations
T1ON	$v_{ce1} = V_{ce}^{sat}$ $v_1 = V_{dc} - v_{ce1}$ $v_{d2} = -k(v_1 - r_s i_1) - (1-k)\omega_r \frac{d\lambda_m}{d\theta_r} - V_{dc}$ $v_2 = V_{dc} + v_{d2}$
T1COMM	$v_2 = V_{dc} - V_b$ $v_c = V_{dc} + k(v_2 - r_s i_2) - (1-k)\omega_r \frac{d\lambda_m}{d\theta_r}$ $v_{d1} = r_s i_1(0) \frac{e^{-r_s h/L_c}}{1 - e^{-r_s h/L_c}} - v_c$ if $v_{d1} < -V_z$ then $v_{d1} = -V_z$ $v_1 = V_{dc} + v_{d1}$
T2ON	$v_{ce2} = V_{ce}^{sat}$ $v_2 = V_{dc} - v_{ce2}$ $v_{d1} = -k(v_2 - r_s i_2) + (1-k)\omega_r \frac{d\lambda_m}{d\theta_r} - V_{dc}$ $v_1 = V_{dc} + v_{d2}$
T2COMM	$v_1 = V_{dc} - V_b$ $v_c = V_{dc} + k(v_1 - r_s i_1) + (1-k)\omega_r \frac{d\lambda_m}{d\theta_r}$ $v_{d2} = r_s i_2(0) \frac{e^{-r_s h/L_c}}{1 - e^{-r_s h/L_c}} - v_c$ if $v_{d2} < -V_z$ then $v_{d2} = -V_z$ $v_2 = V_{dc} + v_{d2}$

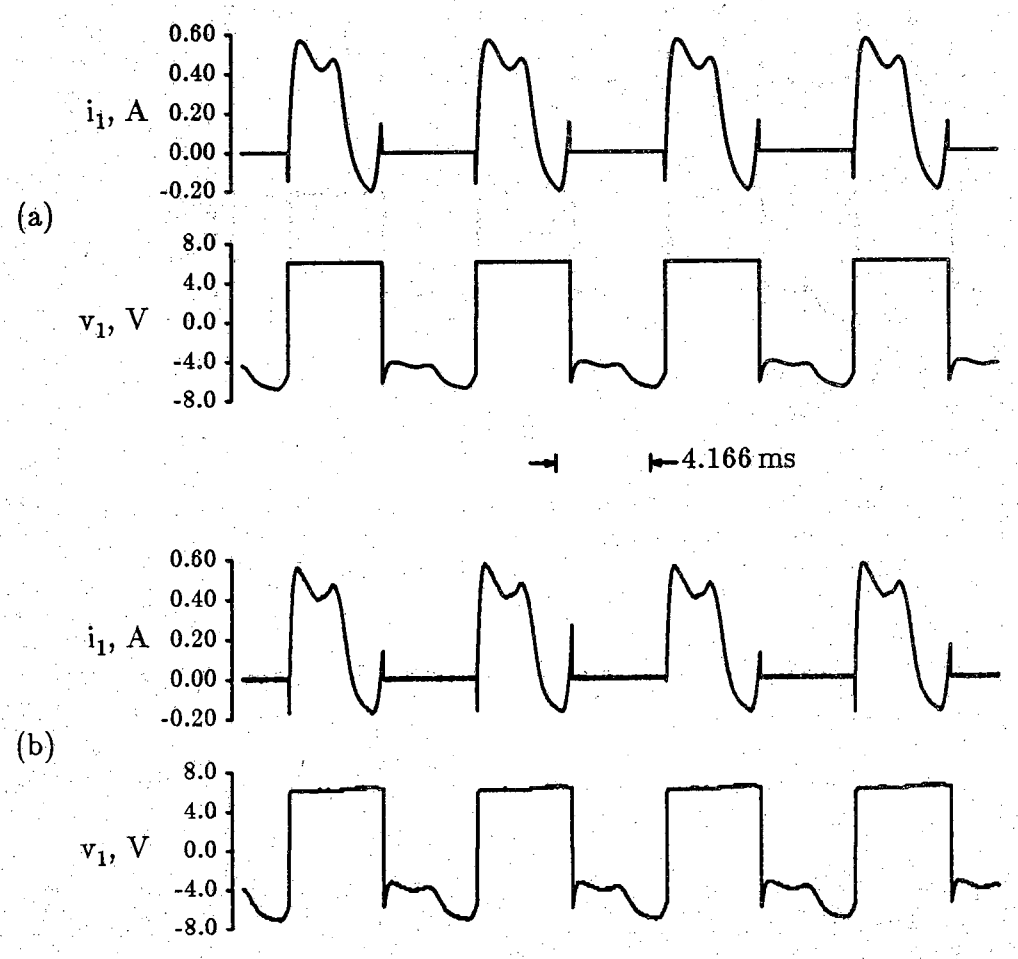

Figure 5.5—1 Comparison of traces from (a) simulation using functional representation and (b) experimental measurement, for a motor operating at $\omega_r = 754$ rad/s and $T_L = 0$.

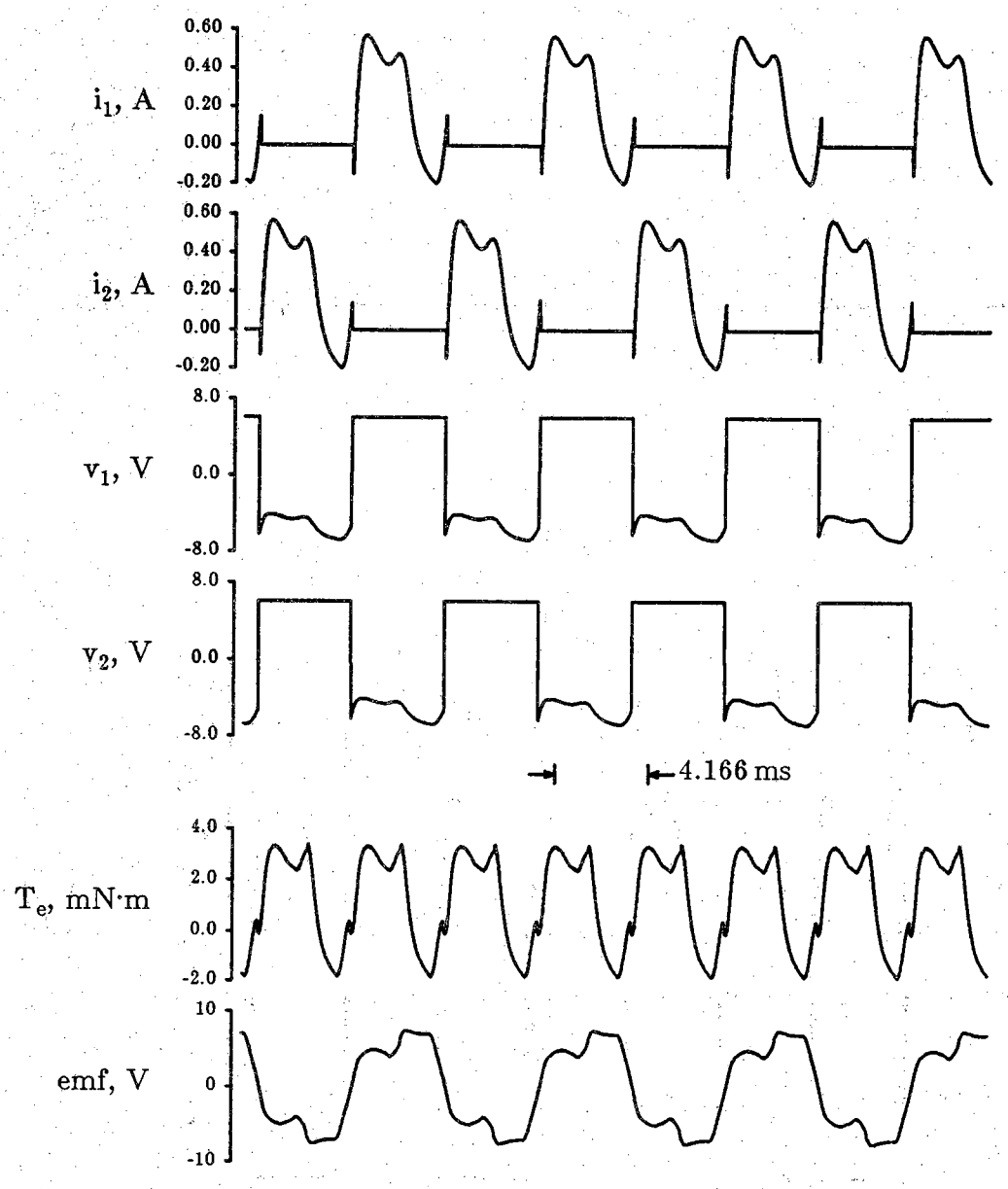

Figure 5.5—2 Functional representation simulation results for a motor operating at $\omega_r = 754$ rad/s and $T_L = 0$.

CHAPTER 6
STEADY-STATE AND DYNAMIC SIMULATIONS

6.1 Introduction

The pulsating starting torque and large moment of inertia of the single-phase brushless dc motor make it impractical for position-control or fast-response speed-control applications. The motor is, however, well suited for constant-speed (steady-state) operation. In this chapter, steady-state operation of the motor is investigated using data produced by computer simulation. In particular, a family of steady-state torque-speed and current-speed characteristics are generated. From these characteristics, the normal operating point for the motor is determined. Operation near this point is then simulated, and the motor efficiency is determined. Finally, the computer simulation is used to demonstrate the dynamic performance of the motor during starting.

6.2 Steady-State Characteristics

In order to investigate the steady-state performance of the motor, electromagnetic torque-speed (T_e–ω_r) and current-speed (I_1–ω_r) characteristics were generated using the computer simulation described in Chapter 5. Here, I_1 represents the average current in the 1-winding and T_e is the average torque.

Families of the simulated T_e—ω_r and I_1—ω_r characteristics are depicted in Fig. 6.2—1 and Fig. 6.2—2, respectively. The families consist of curves corresponding to dc supply voltages ranging from 4 V to 12 V. Each curve was generated by simulating the motor at several constant rotor speeds (electrical angular frequencies) ranging from 20 rad/s to 1200 rad/s and recording the average electromagnetic torque and 1-winding current during one revolution. The functional representation of the inverter was used in the simulations in order to reduce computation time; even so, this procedure for generating the characteristics was computationally intensive.

The torque-speed characteristics in Fig. 6.2—1 are typical of a brushless dc motor. In particular, the slopes of the curves are negative throughout the region where rotor speed and electromagnetic torque are both positive (motor action), and, at rotor speeds between stall and 377 rad/s, the characteristics are nearly linear. The upward concavity for speeds above 377 rad/s is attributable to commutation effects which become more prominent at higher speeds (larger number of commutations per unit time).

Using the family of T_e—ω_r characteristics and manufacturer's specifications for running torque, the normal operating voltage for the motor was established. The running torque is the combination of load torque, T_L, and the windage and friction torque which is modeled as $B\omega_r$. Manufacturer's specifications provided the normal running torque as 4.9 mN·m and rotor speed (electrical angular frequency) as 754 rad/s. In the steady state, the torque due to inertial acceleration can be neglected and the electromagnetic torque developed by the motor counters only the running torque. Thus, the point on the T_e—ω_r characteristic whose ordinate is $T_e = 4.9$ mN·m and abscissa is

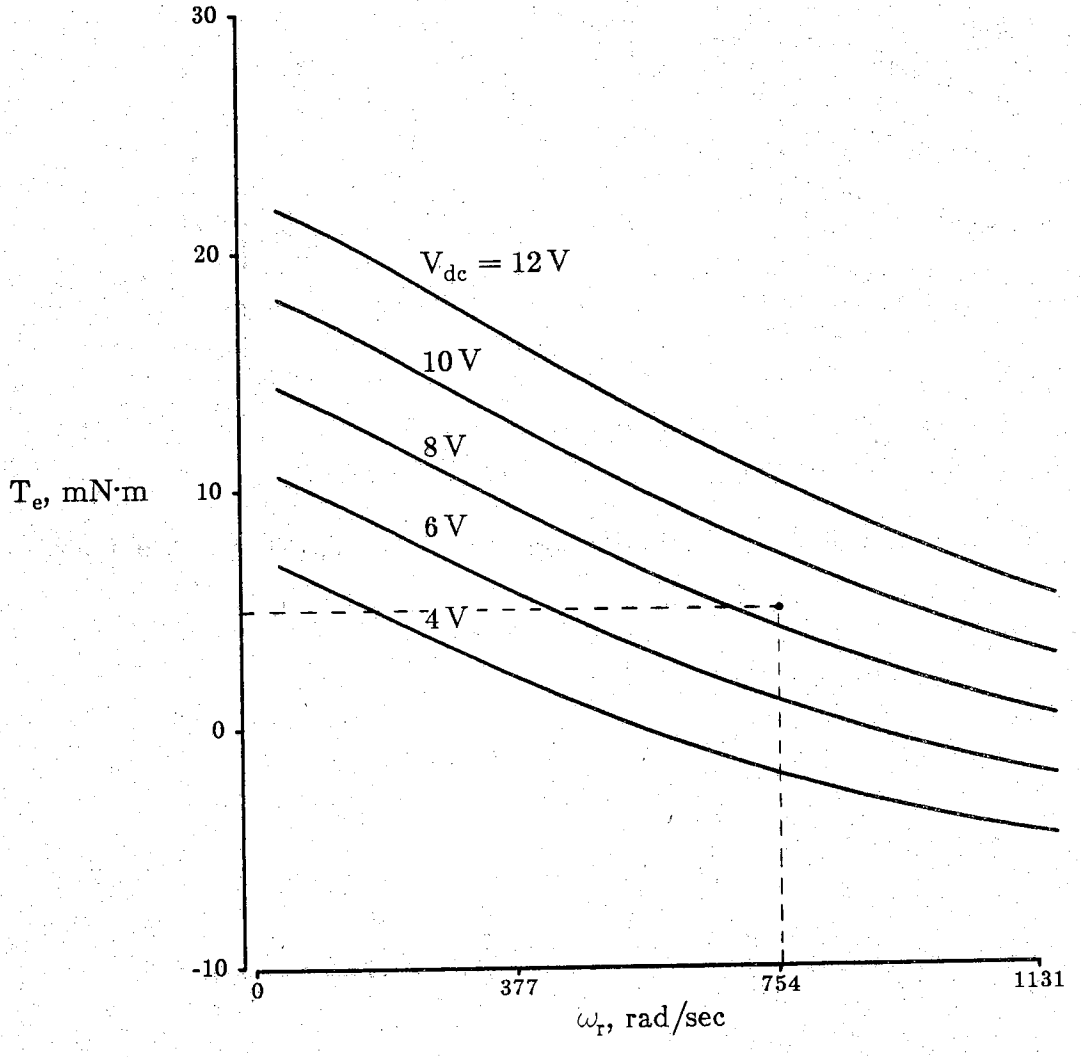

Figure 6.2–1 Torque-speed characteristics for $V_{dc} = 4, 6, 8, 10,$ and 12 V.

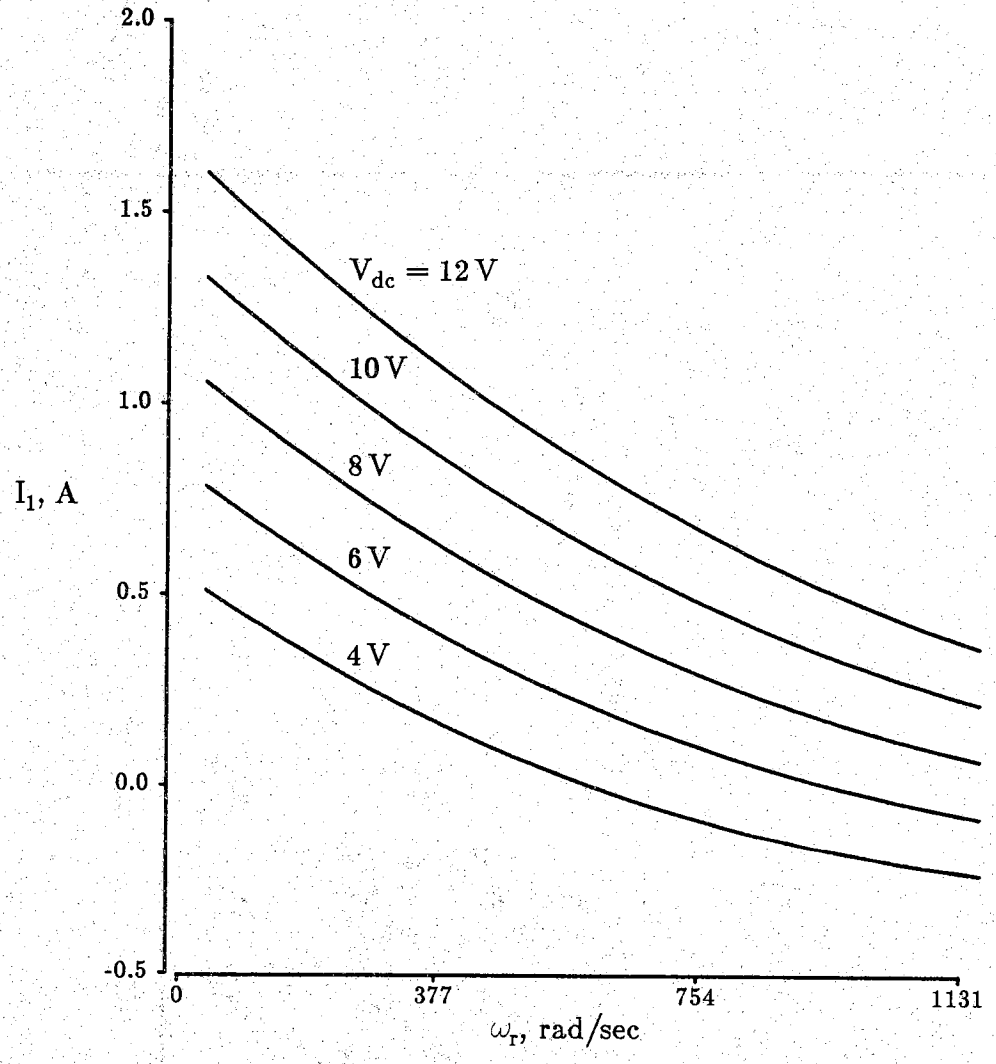

Figure 6.2—2 Current-speed characteristics for $V_{dc} = 4, 6, 8, 10,$ and 12 V.

$\omega_r = 754\,\text{rad/s}$ corresponds to the normal operating point of the motor. This point is indicated in Fig. 6.2—1. The dc supply voltage (applied stator winding voltages) required for the motor to develop $4.9\,\text{mN·m}$ at $754\,\text{rad/s}$ was estimated as $8.3\,\text{V}$ by interpolation between the 8 and $10\,\text{V}$ curves in Fig. 6.2—1. In practice, the applied stator winding voltages would be regulated to maintain the appropriate operating point (rotor speed). That is, pulse width modulation (PWM) would be employed to reduce a dc supply voltage of $12\,\text{V}$ to an effective applied stator winding voltage of $8.3\,\text{V}$. Voltage reduction through PWM is achieved by periodically switching the applied voltage to zero, thereby reducing its average value. The length of time that zero voltage is applied would be determined from a comparison of the measured rotor speed with a reference speed. For purposes of simulation, however, it is assumed that the dc supply voltage has been set to a constant value of $8.3\,\text{V}$ and PWM is not considered.

The motor operating at $\omega_r = 754\,\text{rad/s}$ with $V_{dc} = 8.3\,\text{V}$ was simulated with the inverter switching elements modeled by their I-V characteristics. Resulting traces of the machine variables are given in Fig. 6.2—3. The most notable aspects of the traces pertain to the winding currents. In particular, it is noted that at the instant the winding currents are commutated, the value of the two currents are nearly equal in magnitude but opposite in sign. Considering the commutation of the winding current from the 1-winding to the 2-winding, i_2 is zero prior to commutation and the flux linking both windings is related only to i_1 and the rotor permanent magnets. During the commutation interval, i_1 decreases rapidly. But because the winding flux linkages have a tendency to remain nearly constant throughout the commutation interval, the

decrease in i_1 requires a corresponding (negative) increase in i_2. The increase in i_2 must have a negative sense because the mutual inductance is negative. The forward-biased diode connected to the 2-winding provides the conduction path for i_2. After the commutation interval, i_2 increases under the influence of the applied stator voltage, v_2, until the instantaneous back emf counters v_2. The instantaneous current, i_2, decreases as the back emf reaches a maximum during the latter part of the cycle. After reaching a maximum, the back emf decreases and i_2 again increases rapidly immediately prior to commutation. At commutation, the cycle begins to repeat for the 1-winding current.

In addition to traces of the instantaneous machine variables for motor operation at $\omega_r = 754\,\text{rad/s}$, torque-speed and current-speed characteristics for $V_{dc} = 8.3\,\text{V}$ were generated. These characteristics are given in Fig. 6.2—4. From these data, a plot of motor efficiency, η, versus rotor speed can be obtained using the relationship

$$\eta = \frac{P_{out}}{P_{in}} \tag{6.2-1}$$

where P_{in} and P_{out} are the average input and output power, respectively. For the brushless dc motor, the average input power is the product of the dc supply voltage (constant) and the average dc current drawn by motor. The average dc current is obtained by doubling the 1-winding current, I_1, to account for the second winding. The output power of the motor is the product of electromagnetic torque with rotor mechanical speed. Because the motor is a four-pole device, the rotor mechanical speed is equal to one-half the electrical angular speed, i.e. $\frac{1}{2}\omega_r$. Thus, the expression for efficiency becomes

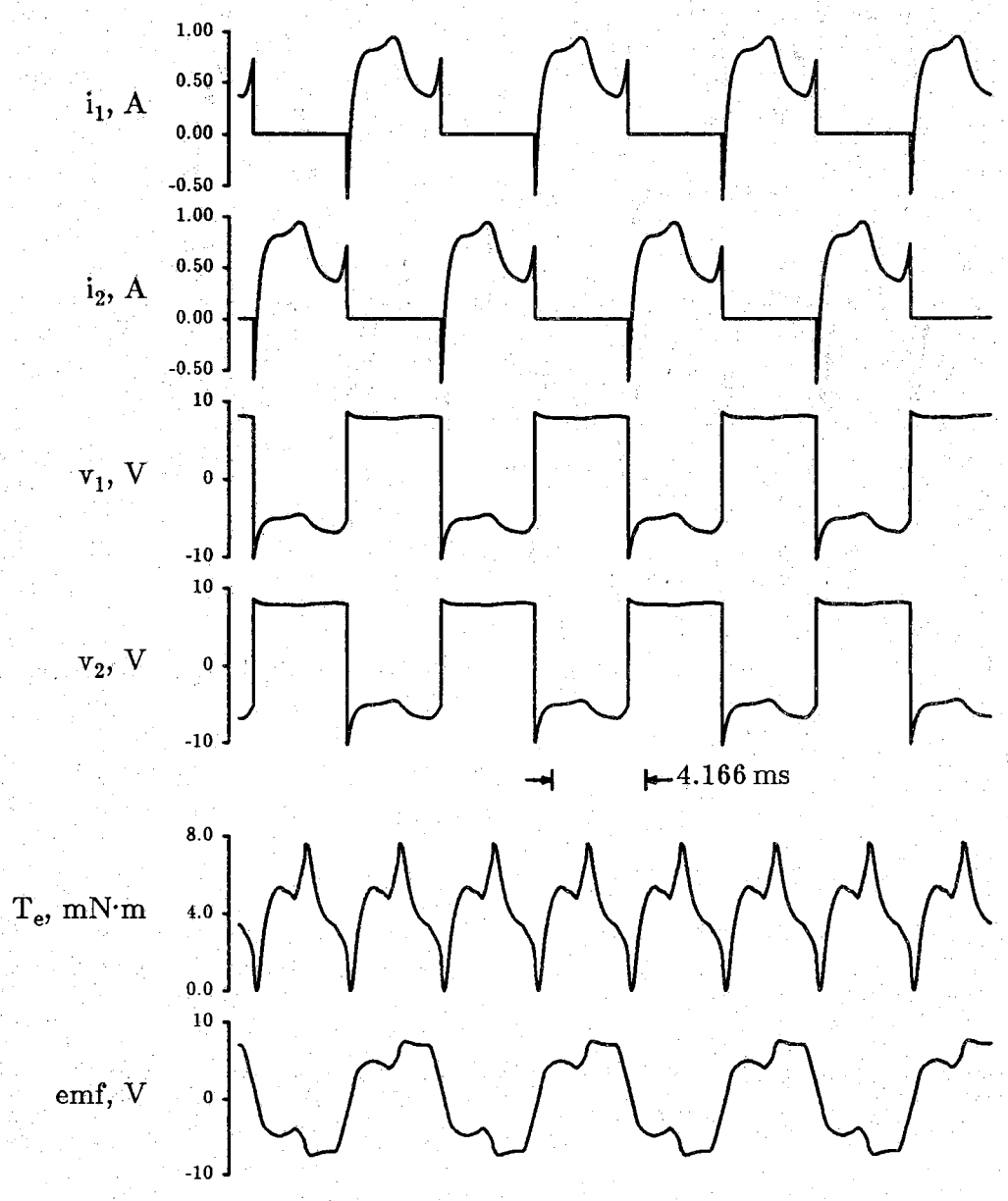

Figure 6.2—3 Machine variables for motor operating with $\omega_r = 754\,\text{rad/s}$ and $V_{dc} = 8.3\,\text{V}$.

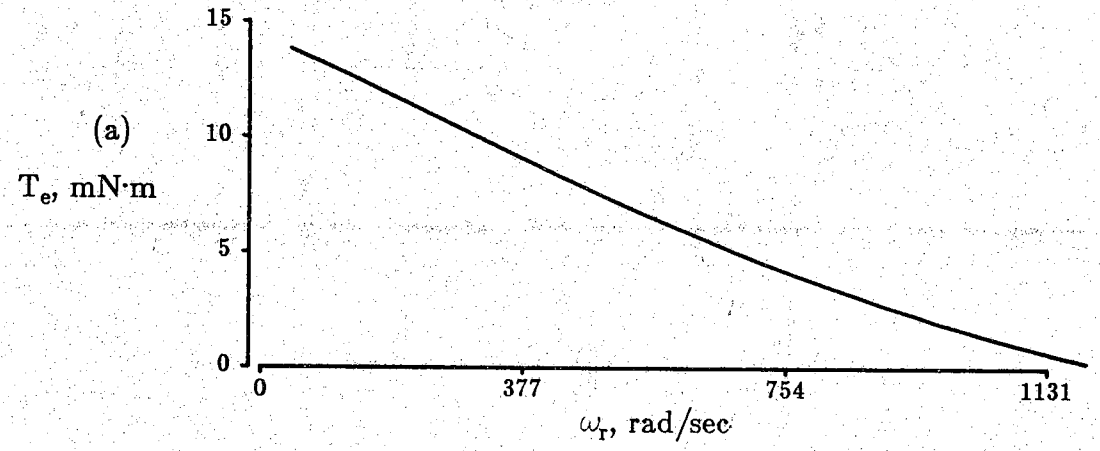

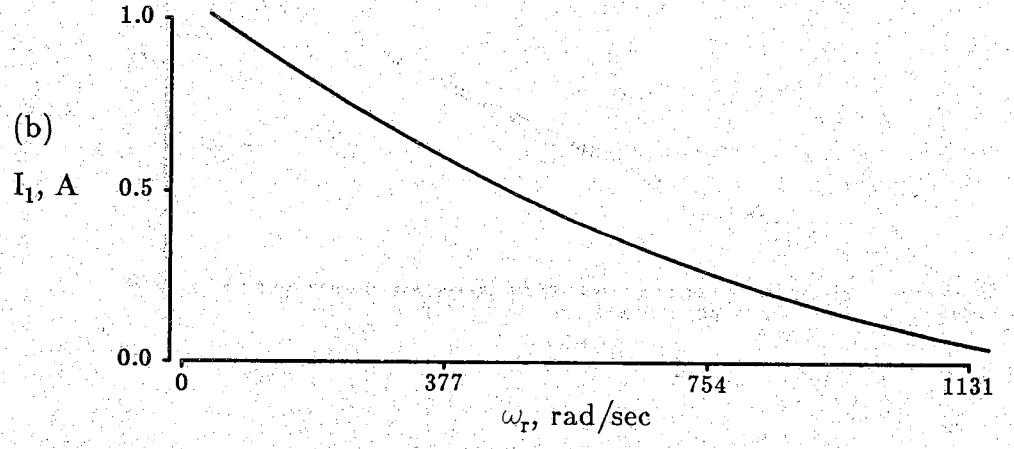

Figure 6.2–4 Characteristics for $V_{dc} = 8.3\,V$ (a) T_e–ω_r and (b) I_1–ω_r.

$$\eta = \frac{\frac{1}{2}T_e\omega_r}{2V_{dc}I_1} = \frac{1}{4}\frac{T_e\omega_r}{V_{dc}I_1} \qquad (6.2\text{-}2)$$

Using (6.2-2) and the data from Fig. 6.2–4, the plot of efficiency given in Fig. 6.2–5 was produced. The motor has an efficiency of 0.34 at $\omega_r = 754$ rad/s, while a maximum efficiency of 0.37 is achieved around $\omega_r = 900$ rad/s.

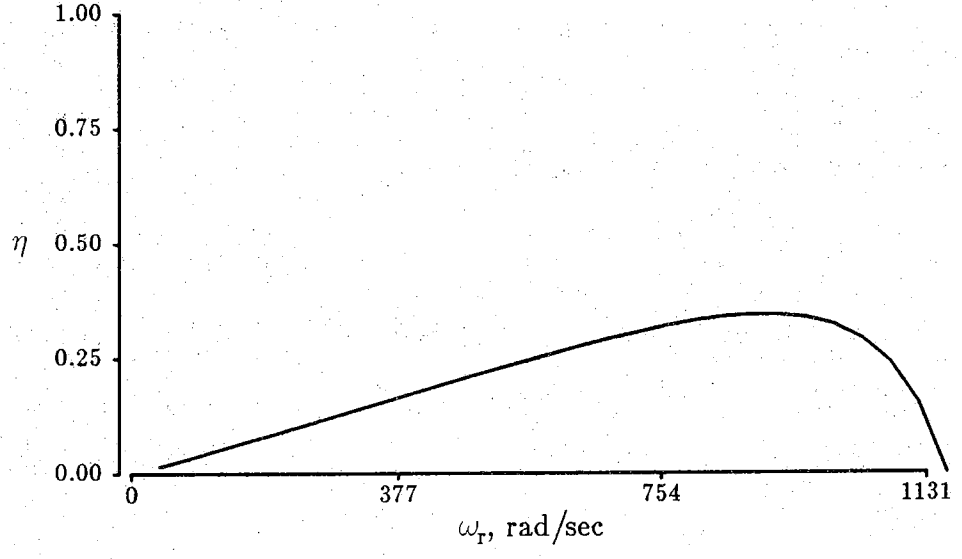

Figure 6.2–5 Plot of motor efficiency for $V_{dc} = 8.3$ V.

6.3 Starting Characteristics

The starting characteristics analyzed in Chapter 4 can be demonstrated using the computer simulation of the motor. In order to accurately simulate the starting characteristics, the cogging torque, which was omitted from the

expression for electromagnetic torque, is represented here as a position dependent load torque. In particular, the form of the load torque is given by

$$T_L = 11 \sin(2\theta_r - 44^\circ) \quad \text{mN·m} \tag{6.3-1}$$

where 11 mN·m is the maximum cogging torque. The argument of sine function in (6.3-1) follows directly from the plot of cogging torque in Fig. 4.3—2. The rotor position must be initialized to a stable detent; the value $\theta_r = 292^\circ$ is used. All other state variables are initialized to zero. During starting of the actual motor, a maximum voltage of 12 V is applied to the stator windings, and in the simulation $V_{dc} = 12$ V. The proportionality constant, B, for the windage and friction torque was calculated as 6.5 μN·m·s by dividing the manufacturer specified running torque by the specified rotor speed. Using these data, the dynamic performance of the motor during starting was simulated. Resulting traces of machine variables are given in Fig. 6.3—1.

These traces demonstrate many of the features hypothesized during the analysis of the starting characteristics in Chapter 4. In particular, for the first several revolutions after energizing the motor, the winding currents are nearly rectangular and the the electromagnetic torque developed by the motor resembles the derived static electromagnetic torque. The algebraic sum of the electromagnetic, load, windage, and friction torques is labeled as T_{net} in Fig. 6.3.1. The net torque remains positive at all rotor positions and the motor has a continuously positive acceleration.

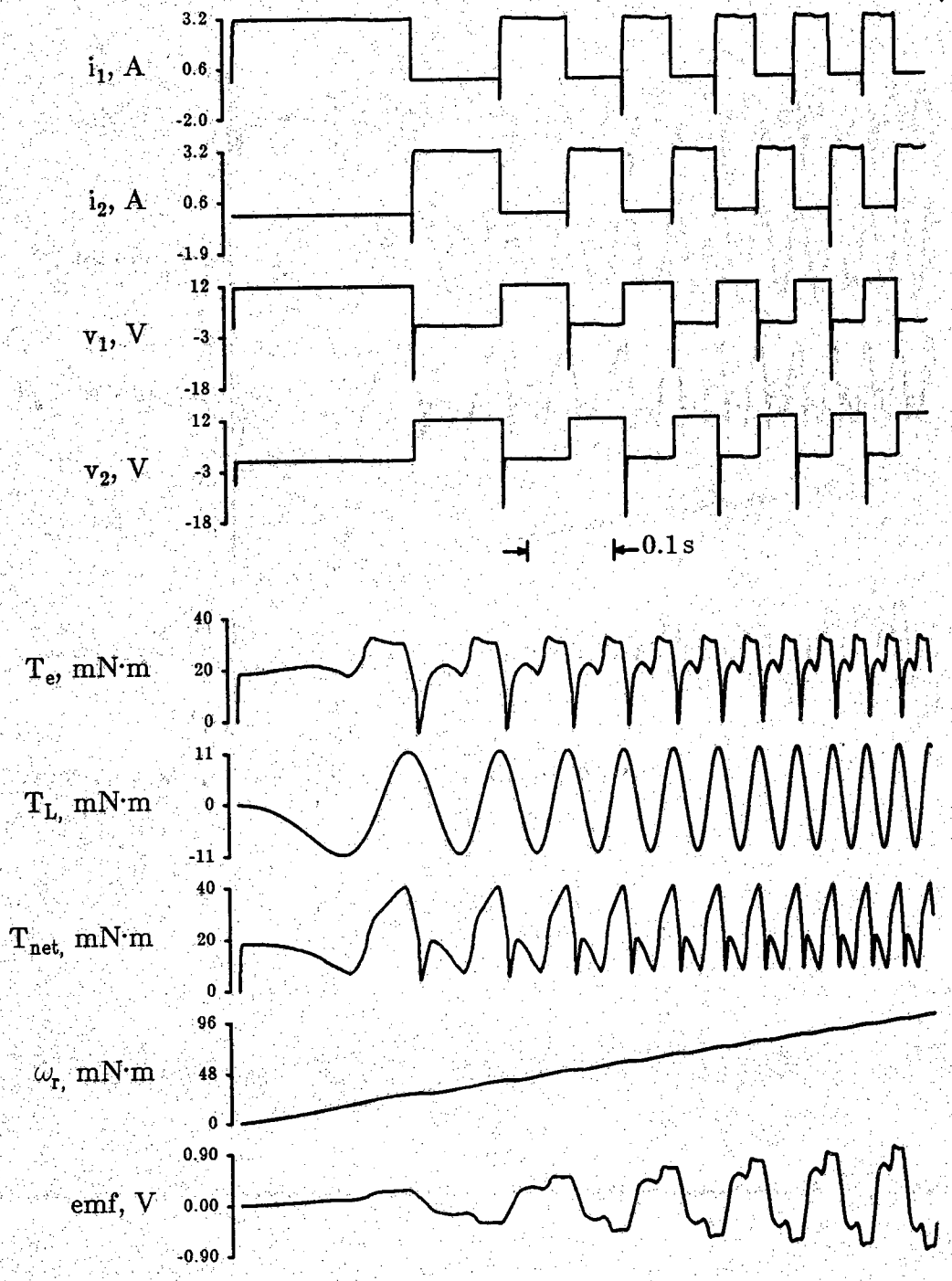

Figure 6.3–1 Machine variables during starting.

CHAPTER 7
SUMMARY AND CONCLUSIONS

In this thesis, models of the permanent-magnet synchronous machine and dc-to-ac inverter which comprise a single-phase brushless dc motor have been developed. Central to the model of the brushless dc motor is the form of the synchronous machine's stator winding flux linkage due to the rotor permanent magnets. The permanent-magnet component of stator flux linkage has been derived analytically and compared with measured results revealing excellent agreement. Two different mathematical models of the dc-to-ac inverter have been established: one in which the current-voltage characteristics of the inverter switching elements are incorporated; the second is a reduced model which permits a more efficient computer simulation. Operation of the brushless dc motor was simulated using each inverter model. Comparison of simulation results with measurements of an actual motor-inverter system indicate that the computer models are very accurate.

The starting response of the motor was analyzed using static electromagnetic torque and cogging torque characteristics. The cogging torque results from variations in the stator reluctance with respect to rotor position and is accentuated intentionally by the asymmetry of the stator pole faces. The cogging torque acts to drive the unexcited motor to a position at which

sufficient (static) electromagnetic torque is developed upon energization to accelerate the motor. This method of ensuring that the motor develops sufficient starting torque is well suited for the single-phase brushless dc motor.

LIST OF REFERENCES

LIST OF REFERENCES

[1] Takashi Kenjo, *Permanent-Magnet and Brushless DC Motors* , Caledon Press, 1985.

[2] M. R. Harris, "Brushless Motors - A Selective Review," Proc. First European Conference on Electrical Drives, Motors, and Controls pp. 84-90, July 1982.

[3] Paul C. Krause, *Analysis of Electric Machinery* , McGraw Hill, 1986.

[4] Raymond DeCarlo, Class notes, 1987.

[5] James S. Vandergraft, *Introduction to Numerical Computations* , Academic Press, 1978.

[6] William H. Hayt Jr. and Gerold W. Neudeck, *Electronic Circuit Analysis and Design* , Houghton Mifflin Co., 1984.